POLITECNICO DI MILANO

School of Industrial and Information Engineering
Department of Aerospace Science and Technology
Master of Science in Space Engineering

Master Thesis

Interface between the long-term propagation and the destructive re-entry phases exploiting the overshoot boundary: the case of INTEGRAL

Supervisor: Prof. Camilla Colombo
Co-supervisor: Dr. Mirko Trisolini

Student:
Christian Fusaro
matricola 928027

Academic Year 2020/2021

This content is original, written by the Author, Christian Fusaro. All the non-originals information, taken from previous works, are specified and recorded in the Bibliography.

When referring to this work, full bibliographic details must be given, i.e.

Christian Fusaro, "Interface between the long-term propagation and the destructive re-entry phases exploiting the overshoot boundary: the case of INTEGRAL". 2021, Politecnico di Milano, Faculty of Industrial Engineering, Department of Aerospace Science and Technologies, Master in Space Engineering, Supervisor: Camilla Colombo, Co-supervisor: Mirko Trisolini

Printed in Italy

Aknowledgments

Part of the journey is the end.
- Tony Stark

First of all I would thank my thesis supervisor Professor Camilla Colombo and my correlator Dr Mirko Trisolini for all the support they gave me during the months dedicated to the development of this thesis. I want to thank them for the infinite patience demonstrated, giving me always professional indications.

A big thank you goes to all the friends met during these years in Milan. Naming all of them would be impossible, but thank you for all the moments spent together during this experience and thank you for making me immediately feel at home.

A special thank goes to my parents, for always believing in me. Thanks to support me in front of every difficulty. Without you this would not have been possible.

Thank you to my brother, for teaching me that calm and determination are the keys to reach even the most difficult of the goals.

Finally, a thank you goes to my friends in Merano that despite being far away have always been close to me.

Summary

The constant increase of the density of satellites in the space environment has lead to the need for investigating technologies able to remove non-operative systems from the Earth's orbit, with the objective to comply with the current guidelines that define the maximum admissible risks and to mitigate the probability associated to collisions in orbit. During the years several studies have been focused on the development of active and passive strategies to remove systems from the space environment.

The present work investigates the feasibility to develop a reliable approach to analyse the re-entry strategy of a satellite. The numerical model shall be able to interface the long-term orbit propagation obtained through semi-analytical methods with the atmospheric re-entry phase exploiting the overshoot boundary concept.

The goal of the thesis is to develop a general method that can be applied to different cases in order to provide a fast way to analyse the atmospheric re-entry of a satellite, searching the correct balance between approximation and precision. The proposed method allows us to compute quickly the conditions at the entry interface and can therefore provide a comparison between different disposal strategies.

The model is then used in this thesis to analyse the atmospheric re-entry of INTEGRAL and to estimate the characteristics that define the destructive re-entry phase. In particular the focus is on the reliability of the method, analysing the influence that an area-to-mass ratio vari-

ation can have on it and on how uncertainty effects can influence the re-entry trajectory of the spacecraft.
The interface conditions, computed exploiting the overshoot boundary concept and taking into account a possible break-off of the solar panels, are used to estimate the destructive re-entry phase using simplified expressions to quantify the loads that are affecting the spacecraft during the re-entry.
The method developed for the analysis of the re-entry trajectory of a space system is characterised by a low computational cost and can be used to perform a quick comparison between different end-of-life strategies. This thesis was part of the COMPASS project: "Control for orbit manoeuvring by surfing through orbit perturbations" (Grant agreement No 679086). This project is a European Research Council (ERC) funded project under the European Union's Horizon 2020 research (www.compass.polimi.it).

Keywords: End-of-life disposal, HEO, Overshoot boundary, Re-entry predictions

Sommario

Il continuo aumento della densitá di satelliti nell'ambiente spaziale rende sempre piú significativo lo studio di tecnologie in grado di rimuovere sistemi non-operativi dall'orbita terrestre, allo scopo di rispettare le linee guida che definiscono gli standard di sicurezza e di mitigare il rischio di collisioni in orbita. Nel corso degli anni vari studi sono stati incentrati sullo sviluppo di metodi di rimozione di sistemi dall'ambiente spaziale e hanno portato allo sviluppo di differenti strategie sia attive che passive.
Il presente lavoro investiga la possibilitá di sviluppare un approccio affidabile per analizzare la strategia di rientro di un satellite. Il modello deve essere in grado di interfacciare la propagazione sul lungo termine degli elementi orbitali con la fase di rientro distruttivo nell'atmosfera terrestre sfruttando il concetto di overshoot boundary.
Lo scopo della tesi é quello di creare un modello generale applicabile a diversi casi in modo da fornire un metodo rapido per l'analisi della strategia di rientro di un satellite cercando il giusto equilibrio tra approssimazione e precisione. Il metodo proposto permette di ricavare rapidamente le condizioni all'interfaccia con l'atmosfera terrestre e rende quindi possibile il confronto tra i rientri distruttivi relativi a diverse strategie.
Il metodo viene applicato in questa tesi per analizzare il rientro atmosferico di INTEGRAL e per stimare le caratteristiche fondamentali che caratterizzano il rientro distruttivo. In particolare, viene studiata la

dipendenza del metodo applicato dal rapporto area-massa del veicolo e dalle condizioni iniziali dell'orbita, tenendo conto di possibili incertezze sulla manovra di disposal.
Le condizioni all'interfaccia, calcolate sfruttando il concetto di overshoot boundary e tenendo conto di un eventuale distacco dei pannelli solari che puó avvenire prima del rientro atmosferico, vengono utilizzate come condizioni iniziali per stimare, attraverso equazioni semplificate, i carichi a cui é sottoposto il satellite durante il rientro.
Il modello sviluppato mantiene un basso costo computazionale e si presta quindi ad essere utilizzato come strumento di confronto rapido tra diverse strategie di fine vita di una missione spaziale. Questa tesi é parte del progetto COMPASS: "Control for orbit manoeuvring by surfing through orbit perturbations" (Grant agreement No 679086). Questo progetto é un progetto finanziato dall'European Research Council (ERC) nell'ambito della ricerca European Unions Horizon 2020 (www.compass.polimi.it).

Parole chiave: Rientro a fine vita, HEO, Overshoot boundary, Previsione di rientro

Contents

1 Introduction **1**

1.1 Aim of the thesis 1

1.2 State of the art 3

1.2.1 Long-term propagation 3

1.2.2 Post-missions disposal guidelines 5

1.2.3 Disposal design and re-entry predictions 7

1.2.4 Demisability analysis 10

1.2.5 Orbit propagation and re-entry phase interface . 11

1.3 Thesis Outline 13

2 Long-term propagation **15**

2.1 Reference frames 15

2.1.1 Earth-centered inertial frame 16

2.1.2 Velocity reference frame 16

2.2 Two-body problem 18

2.3 Perturbed two-body problem 21

2.4 Lagrange's planetary equations 23

2.5 Gauss' form of the variational equations 25

2.6 Perturbations 27

2.6.1 Earth gravity field 27

2.6.2 Third-body perturbation 28

3 Atmospheric interface **31**
3.1 Overshoot boundary 32
3.2 Unified theory 36

4 INTEGRAL Re-entry prediction **41**
4.1 Mission overview 41
4.2 Disposal strategy 43
4.3 Re-entry estimation exploiting the overshoot boundary theory 47
4.3.1 Characteristics of INTEGRAL 47
4.3.2 Drag coefficient 48
4.3.3 Methodology 50
4.3.4 Entry estimation 52
4.4 Area-to-mass ratio variation 54
4.5 Uncertainty analysis 58
4.5.1 Constant area-to-mass ratio 58
4.5.2 Solar panels break-off 65

5 Atmospheric flight **71**
5.1 Final leg 71
5.2 Mechanical and thermal loads 75
5.3 Break-up altitude 79
5.4 Re-entry overview 81

6 Conclusions and future applications **83**

List of Figures

1.1 Object count evolution by object type from Space Environment Statistics by ESA [17] 7

2.1 Earth-Centered Inertial reference frame (XYZ) [31] . . 17
2.2 Normalised perturbative acceleration as function of the spacecraft altitude [35] 22

3.1 Atmospheric Entry Conditions [1] 33
3.2 Entry Corridor [1] 35
3.3 Overshoot Boundary computed for Ballistic Entry ($C_L/C_D = 0$ into Earth's atmosphere ($\bar{\beta}r = 900$). The result is obtained considering a deceleration ratio $f = 0.05$. 40

4.1 Exploded diagram of the INTEGRAL spacecraft. Payload module (upper part) and service module (lower part) [2]. 42
4.2 Perigee altitude evolution of INTEGRAL. The black line depicts the natural perigee evolution over 30 years. The blue line shows how the long-term evolution after the disposal manoeuvre leads to the atmospheric entry of INTEGRAL. 45
4.3 Orbital elements evolution. Natural evolution of INTEGRAL (black line) and disposal strategy (blue line). . . 46
4.4 INTEGRAL: Satellite Configuration in Orbit [41]. . . . 48

4.5 Drag coefficient function of the Knudsen number in the transition regime. The continuous line depicts the trend of the drag coefficient for different geometries of the spacecraft. The dotted line represents the constant approximation adopted for the expression of the coefficient. 50
4.6 Comparison of the final part of the disposal trajectory with the overshoot boundary. The blue cross represents the first time instant when the spacecraft velocity drops below the overshoot boundary. 53
4.7 Final part of the disposal trajectory. Comparison between the trend of u_e for $(S/m)_{MAX}$ and $(S/m)_{MIN}$ and the overshoot boundary. 56
4.8 True anomaly at entry interface for $(S/m)_{MAX}$ (dashed line) and $(S/m)_{MIN}$ (dotted line). 56
4.9 Impulsive velocity variation (Δv), in-plane (α) and out-of-plane angles (β)in the $\hat{\mathbf{t}}, \hat{\mathbf{n}}, \hat{\mathbf{h}}$ reference frame. 59
4.10 Distribution of manoeuvre characteristics affected by uncertainties: 100 test cases. 59
4.11 Perigee evolution of 100 test cases without drag. Target perigee altitude at 50 km. 60
4.12 Distribution of the predicted entry velocity (a) and entry angle (b) for 100 test cases. Entry conditions obtained considering a fixed interface at an altitude of 120 km. . 61
4.13 Distribution of the predicted entry velocity (a) and entry angle (b) for 100 test cases obtained exploiting the overshoot boundary theory as interface method. Prediction obtained considering an area-to-mass ratio value with solar panels (blue) and without solar panels (orange). 63

4.14 Distribution of the predicted entry altitude for 100 test cases obtained exploiting the overshoot boundary theory as interface method. Prediction obtained considering an area-to-mass ratio value with solar panels (blue) and without solar panels (orange). 64
4.15 Distribution of manoeuvre characteristics considering uncertainties on magnitude and manoeuvre angles: 500 test cases. 66
4.16 Overshoot boundary and evolution of the disposal trajectory for 500 test cases. 67
4.17 Entry velocity (a) and entry flight-path angle (b) for 500 test cases obtained exploiting the overshoot boundary theory as interface method and considering a solar panels break-off at 95 km of altitude. 68
4.18 Entry altitude for 500 test cases obtained exploiting the overshoot boundary theory as interface method and considering a solar panels break-off at 95 km of altitude. . 69
4.19 Average number of revolutions with low altitudes passages (below 120 km). 70

5.1 Predicted evolution of the altitude of INTEGRAL with respect to time (a) and downrange (b). Comparison between re-entry estimation obtained with a fixed atmospheric interface (black line) and estimation with the overshoot boundary theory (grey lines). 74
5.2 Predicted evolution of velocity (a) and flight-path angle (b) using a fixed interface altitude (black line) and the overshoot boundary (grey lines) theory as interface methods. 74

5.3 Predicted evolution of the mechanical load acting on INTEGRAL with respect to altitude (a) and time (b) from the entry instant. Trajectories associated to the maximum (red line) and minimum (blue line) peak mechanical accelerations. 77
5.4 Predicted evolution of the thermal flux density acting on INTEGRAL with respect to altitude (a) and time (b) from the entry instant. Trajectories associated to the maximum (red line) and minimum (blue line) peak thermal flux density. 78
5.5 Predicted break-up altitude 80

List of Tables

4.1 Orbital Elements on 2002/11/13 at 00:00. 43
4.2 Magnitude, in- and out-of plane angles and true anomaly of the disposal strategy corresponding to manoeuvre n.5. 44
4.3 Characteristics of INTEGRAL's configuration on orbit. 48
4.4 Area-to-mass ratio values of INTEGRAL 55
4.5 Entry conditions with fixed interface method and overshoot boundary theory for $(S/m)_{MAX}$ and $(S/m)_{MIN}$. . 57
4.6 Integral disposal manoeuvre details [23]. 58
4.7 Mean value and standard deviation of the entry velocity v_e, entry angle γ_e and interface altitude h_e for the different re-entry predictions (fixed interface, overshoot theory with $(S/m)_{MAX}$ and overshoot theory with $(S/m)_{MIN}$. 64
4.8 Average entry conditions. 70

5.1 Integral: re-entry limits 81

Symbols

a	semi-major axis	$[km]$
A_{SP}	solar panels area	$[m^2]$
α	in-plane angle	$[rad]$ or $[deg]$
β	out-of-plane angle	$[rad]$ or $[deg]$
γ	flight-path angle	$[rad]$ or $[deg]$
C_D	drag coefficient	[-]
C_L	lift coefficient	[-]
Δv	velocity variation	$[km/s]$
E	eccentric anomaly	$[rad]$ or $[deg]$
e	eccentricity	[-]
g	gravitational acceleration	$[km\ s^{-2}]$
θ	true anomaly	$[rad]$ or $[deg]$
h	altitude	$[km]$
i	inclination	[-]
J_2	first order zonal harmonics	[-]
$\mathbf{r}$	position vector	$[km]$
$\mathbf{v}$	velocity vector	$[km\ s^{-1}]$
μ	gravitational parameter	$[km^3\ s^{-2}]$
G	universal gravitational constant	$[km^3\ kg^{-1}\ s^{-2}]$
m	mass	$[kg]$
M	mean anomaly	$[rad]$ or $[deg]$
m	mass of the spacecraft	$[kg]$
$\mathbf{\Omega}$	right ascension of the ascending node	$[rad]$ or $[deg]$

ω	argument of perigee	$[rad]$ or $[deg]$
p	semi-latus rectum	$[km]$
ρ	density	$[kg\ m^{-3}]$
σ	bank-angle	$[rad]$ or $[deg]$
S	cross-sectional area of the spacecraft	$[m^2]$
$\oplus$	symbol of the Earth	[-]
$\odot$	symbol of the Sun	[-]
$\mathbb{C}$	symbol of the Moon	[-]

Acronyms

DAS	-	Debris Assessment Software
DOF	-	Degree Of Freedom
DRAMA	-	Debris Risk Assessment and Mitigation Analysis
ECI	-	Earth-Centered Inertial
EOL	-	End-of-life
ESA	-	European Space Agency
GEO	-	Geostationary Orbit
GNSS	-	Global Navigation Satellite System
HEO	-	Highly Elliptical Orbit
INTEGRAL	-	INTErnational Gamma-Ray Astrophysics Laboratory
LEO	-	Low Earth Orbit
NASA	-	National Aeronautics and Space Administration
ORSAT	-	Object Re-entry Survival Analysis Tool
PlanODyn	-	Planetary Orbital Dynamics
SAM	-	Spacecraft Aerothermal Model
SESAM	-	Spacecraft Entry Survival Analysis Module
SCARAB	-	Spacecraft Atmospheric Re-entry and Aero-thermal Breakup
SRP	-	Solar Radiation Pressure
SRV	-	Sample Return Vehicle

Chapter 1

Introduction

The number of satellites in the space environment suffered a rapid increase in the last two decades. The current high density that characterises the orbits around the Earth gives rise to the need of removal methods to guarantee the safety standards necessary for future missions. During the years several works have been focused on the design of end-of-life strategies of space systems.

1.1 Aim of the thesis

The goal of the thesis is to develop a reliable approximated method for the analysis of the disposal strategy of space structures from Highly Elliptical Orbit (HEO), that can be used to perform a quick comparison between different end-of-life strategies, keeping a low computational cost. The model developed connects the long-term orbit propagation obtained through averaged techniques and the destructive re-entry of the spacecraft exploiting the overshoot boundary theory. The overshoot boundary theory proposed in Hicks [1] is used as interface method and is applied at the disposal strategy used to de-orbit the satellite INTEGRAL [2].
The entry condition obtained with the method mentioned above are

then used to obtain an estimation of the destructive re-entry phase of the disposal strategy. The aim is to obtain a complete analysis of the re-entry of INTEGRAL, developing a reliable method that could be applied to different cases.

1.2 State of the art

This section provides an historical overview and a description of the state of the art of the techniques used in the present thesis. Particular attention is brought on the analytical modelling of the perturbation effects on the orbital dynamics. The actual state of the art of the demisability analysis of re-entering structures is presented and in addition are reported the current guidelines that define the post-mission disposal requirements.

1.2.1 Long-term propagation

The motion of an artificial satellite under the effect of orbital perturbations has been intensively studied starting from the second half of the XIX century, due to the wide range of applications that a deep understanding of the orbital motion can have.
The first studies about the analytical modelling of orbit perturbations are addressed by Mikhail L'vovich Lidov and Yoshihide Kozai at the end of the 50's [3] [4]. The first one was a Soviet and Russian astronomer specialised in celestial mechanics [5]. In one of his most important works [3] Lidov gave a significant contribution in the development of mathematical models to describe the orbital propagation in a system composed by Earth and Moon. In these years the same problem was faced by Kozai, a Japanese astronomer known for his studies on orbital motion and secular perturbations. In particular his work developed in 1959 was focused on the effects of Sun and Moon upon the motion of a close Earth satellite under the assumption that the radius of the satellite's orbit is very small compared to that of the Moon [4]. The model was based on the expansion of the disturbing function into a power series of the ratio between the orbital radius and the third body distance. In this work were so developed the terms of the disturbing function related to long-term effects caused by luni-solar perturbations in terms of orbital elements of the satellite, of the Sun

and of the Moon. In one of his later works Kozai developed an alternative model for the calculation of luni-solar perturbations [6]. The disturbing function is written as function of the orbital elements of the satellite and of the polar geocentric coordinates of the Sun and the Moon. In particular the secular effects are computed through numerical integration, while the short period effects are derived analytically. Other works about effects related to the presence of the third body were developed during the following years. In 'Luni-Solar Perturbation of the Orbit of an Earth Satellite' [7] G. E. Cook uses Lagrange's Planetary Equations to obtain the expression of the variation of the orbital elements during a revolution of the satellite and obtains the expressions of the rate of change of the elements. The corresponding expressions are calculated for the effects of solar radiation pressure. Costa and Prado studied the perturbed motion of the satellite when a third body is involved in the dynamics using an analytical double-averaged model, developed in previous works, with the disturbing function expanded using Legendre's polynomial [8]. Particular attention is brought on the effect of the third body perturbation on high-altitude Earth satellites, highlighting under which conditions a near-circular orbit remains near-circular. The model was later on expanded taking into account term up to the eighth order. The influence of the atmospheric drag was derived by King-Hele [9], who derived the averaged equations that define the variation of the semi-major axis and the eccentricity and developed different expressions depending on the orbit eccentricity. Kaufman and Dasenbrock [10] define a semi-analytical method able to analyse the propagation of the orbital elements for lunar and earth orbiters. The model is based on the single averaged equations of motions which are computed in the parallax factor and the mean motion ratio. The single averaged expressions are calculated by considering that the period of the satellite is much lower than the secular characteristic time. In his work the expressions of the third-body disturbing function and its derivatives with respect to the orbital elements are reported up to

the eighth order. Colombo et al. [11] analyse the effects of luni-solar perturbation on Highly Elliptical Orbits, investigating the possibility of exploiting the perturbative effects to design the end-of-life disposal of a spacecraft. The analysis is applied to the INTEGRAL mission, demonstrating that, exploiting the orbital dynamics, an atmospheric re-entry can be obtained with the Δv available on board. The design of end-of-life disposal is further investigated exploiting the construction of maps of the long-term evolution of spacecraft in Highly Elliptical Orbits [12]. The analysis presented allows the identification of initial conditions that, under the effect of luni-solar perturbations, naturally evolve to an atmospheric re-entry. Colombo [13] proposes a Planetary Orbital Dynamics (*PlanODyn*) suite for long term propagation in perturbed environment. *PlanODyn* implements the orbital Earth-centered dynamics written in orbital elements by using semi-analytical averaging techniques. The model is based on the averaged dynamics of the Lagrange or Gauss planetary equation and the semi-analytical approximation for drag is taken from King-Hele [9].

1.2.2 Post-missions disposal guidelines

At the beginning of humans' the space exploration no disposal strategy for the end-of-life of a space mission was planned, leading to an orbital space around the Earth which is now densely populated by satellites that are no more operative.
In Low Earth Orbit (LEO) the disposal of the satellite is simply achieved exploiting the effect of the atmospheric drag, which is able to lead the vehicle to a quick re-entry. In Medium Earth Orbit (MEO), Highly Elliptical Orbit (HEO) and Geostationary Orbit (GEO) the deceleration due to the Earth's atmosphere is no more sufficient to de-orbit the satellite and a proper disposal strategy has to be designed. The uncontrolled long-term evolution of an orbit affected by luni-solar perturbations and by the asymmetry of the gravity field of the Earth can

cause an uncontrolled re-entry of the satellite or bring to an interference with LEO and GEO protected regions.
In order to prevent debris mitigation and to minimise the risk associated to space missions precise guidelines on the post-mission disposal were introduced in more recent years (NASA Handbook [14], ESA Space Debris Mitigation [15] [16]). The objectives of the space debris mitigation policy are to preserve the LEO and GEO protected regions, to prevent debris generation, to avoid orbital collisions by performing collisions avoidance manoeuvres and disposal manoeuvres to limit the presence of non-operational vehicles and to limit the casualty risk on ground associated to controlled and uncontrolled re-entry of space systems. Nowadays the LEO and GEO environment is characterised by the presence of over 10.000 objects with a size of 10 cm or larger, which include operational and non-operational spacecrafts as well as space debris. The 60% of the artificial objects orbiting around Earth is made up of debris generated by fragmentation in orbit [15]. Figure 1.1 depicts the fast increase of the space debris population that occurred in the last decade. The increase was caused by two main fragmentation events:

- In 2009 an US operational communication satellite (Iridium 33, 560 kg) and a Russian decommissioned communications satellite (Cosmos 2251, 900kg) collided at 790 km of altitude, generating more than 2000 catalogued debris in LEO.
- In 2011 a Chinese anti-satellite test involving a satellite destruction (Feng Yun 1C, 957 kg) at 850 km of altitude generated more than 2700 catalogued debris in LEO.

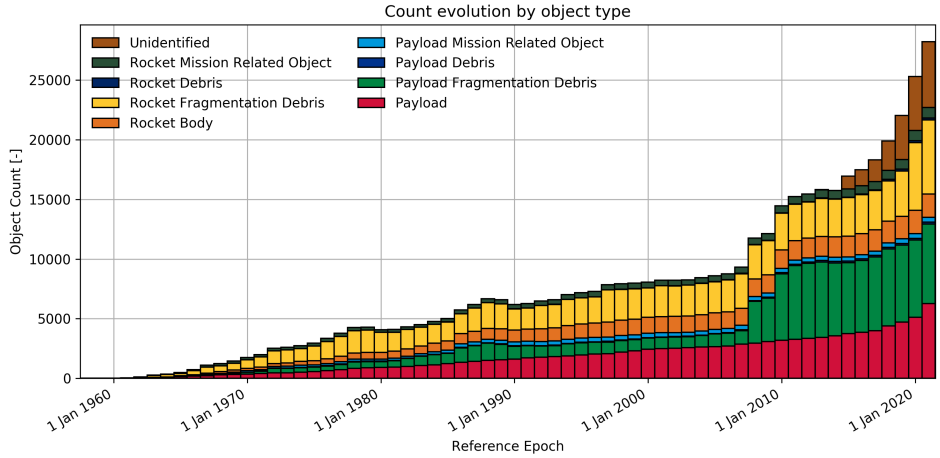

Figure 1.1: Object count evolution by object type from Space Environment Statistics by ESA [17]

No guidelines currently exist for Highly Elliptical Orbit, but the design of manoeuvres with the purpose of removing non-operational vehicles from the space environment is of primary importance to reduce the risk associated to unintentional collisions or uncontrolled re-entries [15].

1.2.3 Disposal design and re-entry predictions

The most complex issue when analysing the disposal strategy of a spacecraft is the identification of the conditions that actually lead to an atmospheric entry. For this reason, a deep investigation in this field has to be performed, in order to develop a method that shall be as reliable as possible.

In 2013 Colombo et al. [18] present a preliminary analysis of possible re-entry strategies for a spacecraft in HEO exploiting the natural evolution of inclination and eccentricity of the orbit under the effects of luni-solar perturbations. The initial orbital conditions of the vehicle define a trajectory in the phase space (2ω,e in the Earth-Moon orbital plane) used to analyse possible re-entry strategies. The purpose is to design a manoeuvre that moves the spacecraft to another trajectory in

the phase space, so that eccentricity fluctuations will lead to a perigee altitude inside the Earth's atmosphere, obtaining the re-entry of the satellite.
In a successive work the study on the End-Of-Life (EOL) disposal of spacecraft in HEO is extended considering the optimisation of the re-entry manoeuvres considering the full dynamical model [11]. The manoeuvre optimisation is obtained exploiting a cost function that takes in account both the minimum reached perigee and the Δv required by the disposal strategy. As a study case the disposal strategy of INTEGRAL is designed for a fixed set of data for the re-entry manoeuvre epoch. It is demonstrated that exploiting the effects of luni-solar perturbations, the fuel available on board is sufficient to obtain the re-entry of the satellite. The strategy adopted depends on the initial conditions of the orbit: if the eccentricity before the manoeuvre is low, the optimised strategy tends to further decrease it, so that the orbital propagation will lead to a higher eccentricity obtaining the re-entry. When the eccentricity is high instead, the optimised strategy tends to further increase it, leading to an atmospheric entry after short time. The orbital dynamics is propagated until a altitude perigee of 50 km is reached. The atmospheric entry conditions (flight-path angle and entry velocity) are then recovered considered a fixed altitude for the Earth's atmosphere at 120 km. The final leg is propagated assuming planar motion and no lift: once the entry trajectory is defined simplified equation [19] are used for a preliminary estimation of the mechanical and thermal loads, from which an estimation of the altitude of fragmentation can be recovered.
The effect of third body perturbation and the asymmetry of the gravity field of the Earth on the stability of HEOs has been further analysed, using averaged expressions for the disturbing potential to propagate the orbital evolution [20]. For each point in the phase space (2ω,e) the maximum variation of eccentricity is computed. This approach allows the construction of maps in the phase space that are used to study the

stability properties of a certain orbit, and particular unstable regions can be exploited to design the end-of-life disposal of the spacecraft.
Nowadays, with the introduction of post-mission disposal guidelines, space activities must be designed to minimise the debris generation and the casualty risk associated to re-entering objects. Armellin et al. [21] [22] present a disposal design method based on the formulation of a multiobjective optimisation problem solved with an evolutionary algorithm. The method is applied either to re-enter the atmosphere of the Earth or to design a manoeuvre that will move the vehicle in a graveyard orbit. With this approach it is possible to obtain an optimisation process that takes into account additional parameters and allows us to maximise the impact latitude (or other requirements) to limit the casualty risk associated to the Earth's re-entry. The multiobjective approach is used as preliminary design method for the disposal of INTEGRAL and for the Galileo satellite using as drivers for the preliminary design robustness, safety and propellant consumption. In particular it is shown how different disposal windows are characterised by different casualty risk levels. Merz et al. [23] report the investigations performed by ESA to influence the long-term orbital evolution that will finally lead to the re-entry of INTEGRAL. The mission has been designed before the post-mission guidelines and the corresponding requirements were introduced by ESA. For this reason the mission is not enforced by post-mission rules. However the long-term propagation shows how the satellite will repeatedly cross protected regions, both in LEO and GEO, without reaching re-entry conditions in the next 200 years. The disposal design strategy considered takes into account the available fuel consumption of the satellite and has the purpose to find a suitable strategy able to extend the operational lifetime of the satellite. The final designed manoeuvre reported in this work is composed by three major burns and a touch-up for final fine-tuning.

1.2.4 Demisability analysis

The re-entry of a spacecraft can be characterised by the presence of surviving fragments, generating a risk to the ground population that can not be neglected. As mentioned above, post-mission guidelines define a maximum acceptable risk associated to re-entering objects. For this reason different re-entry tools have been developed exploiting different approaches to perform the analysis of the destruction process and to obtain an estimation of the on ground risk. Lips and Fritsche [24] compare different re-entry tools to identify their differences. The analysis methods can be divided in two main families:

- object-oriented codes
- spacecraft-oriented codes

Object-oriented codes (DAS, ORSAT, DRAMA/SESAM) introduce a strong simplification in the spacecraft model construction. In all the above mentioned codes the spacecraft model is represented by its individual parts, characterised each by simplified geometry, size, mass and material. The method is based on the assumption that the individual components of the spacecraft are relased at a fixed altitude usually in the range between 75 and 85 km. A spacecraft-oriented code (SCARAB) is instead based on a complete description of the spacecraft, trying to provide a model as close as possible to the real design. Beck et al. present a hybrid approach (SAM) [25]. The destructive re-entry tool mixes different aspects of spacecraft oriented and object oriented codes to obtain a hybrid propagation method. The model propagates the first part of the re-entry trajectory using a 6 DOFs. After the detachment of a component from the main structure, the object dynamics is propagated using a 3 DOFs approach. In 2001 Weaver et al. [26] propose a new probabilistic estimation method of the breakup of reentering space debris, providing distributions of breakup altitude, debris area and casualty area. The approach presented takes into account

uncertainties in the breakup process and highlights their influence in the re-entry phase. All this works show how analysis of the destructive process shall be performed searching for the correct balance between accuracy and reliability.
To conclude, re-entry strategies can be strictly correlated with the design of the spacecraft. Trisolini et al. propose a spacecraft optimisation design based on demise and survivability criteria [27] [28] [29]. Design-for-demise philosophy may encourage uncontrolled re-entry strategies, which are simpler to design, but at the same time the survivability of the spacecraft against accidental debris and meteoroids impact in the space environment must be guaranteed for many years. In order to perform a combined analysis on the demisability and survivability of the spacecraft two models are developed. A simplified spacecraft configuration model for the analysis of the re-entry phase to evaluate the demisability of the vehicle and a second model to perform the analysis of debris impact and obtain a measure of the survivability of the spacecraft. The effect of concurrent requirements on the preliminary design of the spacecraft is provided in a multi-objective optimisation framework. The global purpose is to set the basis for future spacecraft design-for-demise processes, based on the optimisation of more complex spacecraft configurations.

1.2.5 Orbit propagation and re-entry phase interface

Re-entries from HEO are characterised by super-circular entry velocities and entry flight-path angles that are steeper than the entry angles encountered by space systems entering from LEO. Considering that the re-entry from HEO is characterised by high-eccentricities, the entry strategy can present several high-velocity passages in the earth atmosphere that do not allow a capture of the spacecraft. The entry trajectories can be therefore affected by different levels of circularisation

leading the entry conditions to vary over a wide range of values. For this reason the selection of the interface method between the long-term propagation and the destructive re-entry phase can lead to predictions characterised by different entry conditions.
The definition of the entry conditions is usually connected to the definition of a critical target condition. In Colombo et al. [11] the entry conditions are obtained targeting a perigee altitude of 50 km. Below 60 km of altitude the spacecraft is considered in good conditions to achieve the atmospheric re-entry. Once the target perigee altitude is reached, the entry conditions are retrieved computing the conditions of the spacecraft at a fixed entry interface, typically set at an altitude of 120 km. Note that an approach based on this considerations is not taking into account the effects of atmospheric drag that become remarkable in the last part of the orbit propagation. Hicks [1] developed a theory based on the deceleration that the spacecraft encounters during the re-entry trajectory to obtain a prediction of the conditions that can lead to an atmospheric capture of the spacecraft. Trisolini and Colombo [30] used the overshoot theory as interface method between the long term propagation and the destructive re-entry phase for re-entering structures on resonant trajectories from GEO, showing that the concept of overshoot boundary can be a viable method for the prediction of the entry conditions for GEO disposal strategies.

1.3 Thesis Outline

The thesis provides an analysis of the interface between the long-term orbit propagation and the destructive re-entry phases exploiting the concept of overshoot boundary. The work is organised to provide the reader the theory that will be applied in order to perform the interface. The theory presented is then applied at the disposal strategy of INTEGRAL.

Chapter 2 is an overview of the long-term propagation of the trajectory of the satellite. The ideal two-body problem is firstly introduced and then expanded with the introduction of orbital perturbations. Lagrange's Planetary Equations and Gauss' Form of the Variational Equations are presented in order to explain the technique used for the propagation of the orbital elements of the satellite. Particular attention is brought on the method used to model the perturbations associated to the asymmetry of the gravity field of the Earth and to the presence of the third body. Finally the definition of averaged techniques implemented in the *PlanODyn* tool, used for the long-term propagation performed in this work, are introduced.

Chapter 3 presents the method used in this work to interface the long-term propagation with the destructive re-entry phase. The method used to estimate the orbital conditions that lead to an atmospheric-entry is based on the definition of an overshoot boundary following the theory presented in Hicks [1]. The definition of overshoot boundary is presented in the first section and afterwards the unified theory is used to compute the expression of the boundary.

In Chapter 4 the theory presented in the previous chapter is applied to INTEGRAL's disposal orbit propagation in order to define the time instant when the entry conditions are met. The disposal strat-

egy exploited is developed in previous works. The re-entry analysis is firstly carried out for a "nominal" condition. Afterward the re-entry estimation is performed for different set of data considering possible uncertainties on the disposal manoeuvre. The analysis evaluates the influence that the area-to-mass ratio has on the re-entry prediction. The range of the possible entry conditions that characterise the disposal of INTEGRAL is obtained performing an uncertainty analysis over 500 test cases, taking into account a break-off of the solar panels when a passage at a low pre-estabilished altitude occurs. The analysis presents the effects of eventual uncertainties in the impulsive velocity variation on the atmospheric entry conditions.

Chapter 5 uses the re-entry conditions obtained in the previous part of the work to perform an estimation of the atmospheric trajectory of the spacecraft. The re-entry is computed assuming simplified equations for planar motion and no lift. The trajectory obtained under these approximations are used to obtain a preliminary estimation of the mechanical and thermal loads acting on the vehicle and to perform an estimation of the possible break-up altitude of the spacecraft.

Chapter 6 concludes the thesis, summing up the main achievements obtained and provides possible future applications of the method followed in this work.

Chapter 2

Long-term propagation

The design of the end-of-life strategy is a complex task that requires the propagation of the orbital evolution of the spacecraft over a long time. The orbital dynamics is characterised by the presence of several perturbation effects that increase the computational time required to obtain an exact long-term evolution of the orbital elements. The present Chapter introduces a model for the description of the dynamic evolution of the spacecraft based on the Lagrange's Planetary Equations and on the expression of the potential of disturbing effects. The *PlanODyn* tool [13], based on the model that is briefly explained throughout this Chapter, allows us to obtain a propagation of the orbital dynamics over long time in few seconds. All the propagations performed in this work are performed using the above mentioned tool.

2.1 Reference frames

One of the first requirements needed to describe the motion of a satellite in orbit is to define a suitable reference frame, which usually means finding a proper inertial coordinate system. Two different reference frames are used in this work.

2.1.1 Earth-centered inertial frame

In order to describe the orbit of a satellite around the Earth we have to define a suitable reference frame. Earth-based reference frames are typically used. The reference plane used is the equatorial plane with its origin a the centre of the Earth and is defined through three unit vectors XYZ. The X axis directed to the vernal equinox, the Z axis points the direction defined by the North Pole and the Y axis is oriented in the direction that completes the orthogonal tern. Figure 2.1 shows the non-rotating inertial frame of reference XYZ with its origin at the center C of the Earth known as Earth-Centered Inertial frame.

2.1.2 Velocity reference frame

In this system the primary axis N lies in the orbital plane, normal to the velocity vector. The T axis is tangential to the orbit and the H axis is normal to the orbital plane. This reference frame is used mainly to analyse drag effects on the orbit, due to the consideration that drag effects always act along the velocity vector. The velocity reference frame is built as follows

$$\begin{aligned} \hat{\mathbf{t}} &= \frac{\mathbf{v}}{|\mathbf{v}|} \\ \hat{\mathbf{h}} &= \frac{\mathbf{r} \times \mathbf{v}}{|\mathbf{r} \times \mathbf{v}|} \\ \hat{\mathbf{n}} &= \hat{\mathbf{h}} \times \hat{\mathbf{t}} \end{aligned} \tag{2.1}$$

In this work the $\hat{\mathbf{t}}, \hat{\mathbf{n}}, \hat{\mathbf{h}}$ reference frame is used to express the components of the impulsive velocity variation that define the disposal strategy. The components are used to compute the instantaneous variation of the orbital elements through Gauss' form of the variational equations (see Eqs.(2.13)).

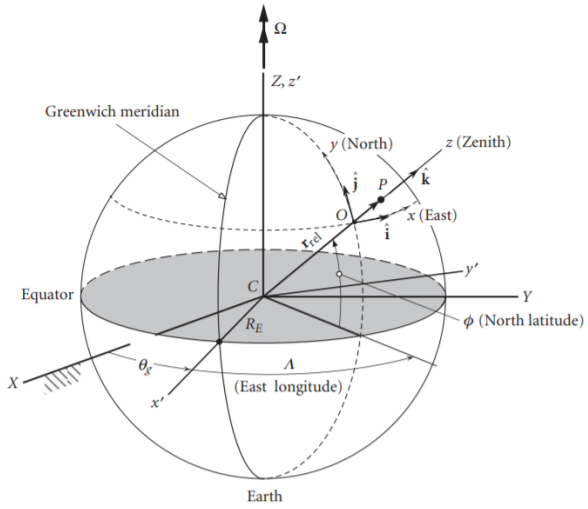

Figure 2.1: Earth-Centered Inertial reference frame (XYZ) [31]

2.2 Two-body problem

The simplest gravitational problem is represented by two point masses. As derived in several works (see Vallado [32], Curtis [31], Battin [33]) the motion of the spacecraft under the influence of the gravity field of a central body is described by the Newton's second law of motion:

$$\ddot{\mathbf{r}} + \mu \frac{\mathbf{r}}{|\mathbf{r}|^3} = \mathbf{0} \tag{2.2}$$

where μ is the gravitational planetary constant and $\mathbf{r}$ and $\ddot{\mathbf{r}}$ are respectively the relative position and the acceleration vector between the two bodies considered. The solution expressed above is obtained under the following assumptions:

- There are only two point masses in space.
- The spherical gravitational fields are the only source of interaction between the two point masses
- The mass of the main attractor is much higher than the mass of the secondary body ($m_0 >> m_1$)

The gravitational parameter is defined as

$$\mu = G(m_0 + m_1) \tag{2.3}$$

where m_0 and m_1 are the mass respectively of the main attractor and the secondary body and G is the universal gravitational constant $G = 6.67 \times 10^{-20}$ km^3/kgs^2.
In all the applications that use the orbital equations for the analysis of the motion of a spacecraft around the Earth, the mass of the secondary body is of several orders of magnitude lower than the main attractor. For this reason the center of mass of the two-body system can be considered to be located at the center of the Earth and the gravitational planetary constant μ can be simplified as

$$\mu_{\oplus} = Gm_{\oplus} \tag{2.4}$$

where $m_{\oplus}$ is the mass of the Earth.For the case of orbit motion around the earth the gravitational parameter is equal to

$$\mu_{\oplus} = 398600 \text{ km}^3/\text{s}^2$$

Eq.(2.2) describing the ideal two-body problem is represented in terms of the relative position vector between the spacecraft and the main attractor.
The equation describes the orbital motion as a function of time and six orbital parameters. The six parameters may be selected as the orbital elements: the semi-major axis a (or alternatively the specific angular momentum h) and the eccentricity e (describing the shape of the orbit), inclination i, longitude of the node Ω, argument of perigee ω and the true anomaly θ (or alternatively the mean anomaly M).
It is often convenient to represent the motion of the spacecraft through the orbital elements. As derived in Curtis [31] the orbit equation can be described as

$$r = \frac{a(1-e^2)}{1+e\cos(\theta)} \tag{2.5}$$

Eq.(2.5) describes the position of the spacecraft around the main attractor as a function of time, relating the radius of the orbit with the true anomaly θ.
The mean anomaly M is connected to the true anomaly θ through the eccentric anomaly E as follows

$$\tan\frac{\theta}{2} = \sqrt{\frac{1+e}{1-e}}\tan\frac{E}{2} \tag{2.6}$$

$$M = E - e \sin E \tag{2.7}$$

2.3 Perturbed two-body problem

Newton's second law describes the ideal motion of the spacecraft around the planet. Any effect that deviates the motion from the ideal trajectory is known as a perturbation.
The most significant perturbations of the two-body motion are related to non-spherical gravity field of the main attractor, atmospheric drag, Solar Radiation Pressure (SRP) and gravitational forces related to the presence of other celestial bodies. Taking into account the presence of perturbations the equation of motion becomes

$$\ddot{\mathbf{r}} = -\mu\frac{\mathbf{r}}{r^3} + \sum \mathbf{a}_p \tag{2.8}$$

where $\mathbf{a}_p$ is any acceleration produced by the acceleration sources, other than the spherical symmetric gravitational attraction between the two bodies.
As shown in Figure 2.2 the perturbation associated to atmospheric drag depends on the atmospheric density and is therefore rapidly increasing for low altitudes. For orbits presenting passages at low altitudes (LEO or HEO) the deceleration due to atmospheric drag is able to de-orbit the satellite.
The dependence of other perturbations on altitude is less significant and is highlighted in Figure 2.2. At 1000 km of altitude, the orders of magnitude of the pertubation effects are [31] [34]

$$\begin{aligned} p_{J_2} &\approx 10^{-2} a_0 \\ p_{\mathbb{C}} &\approx 10^{-7} a_0 \\ p_{SRP} &\approx 10^{-9} a_0 \end{aligned} \tag{2.9}$$

where $a_0 = \mu/r^2$ is the acceleration related to the presence of the

main attractor in an ideal two-body motion and p_{J_2}, $p_{\leftmoon}$ and p_{SRP} are respectively the perturbation effects related to the Earth's oblateness, the lunar gravity and the SRP.
Different works showed that the contribution of luni-solar perturbations is of primary importance in the dynamic evolution of HEO [11][23]. The disposal manoeuvre itself designed to achieve the re-entry of INTEGRAL was obtained exploiting the influence of luni-solar perturbations on the orbit dynamics.
According to these considerations, the long-term evolution of INTEGRAL is computed in this work considering the effects of luni-solar perturbations, of the Earth's oblateness and of the aerodynamic drag.

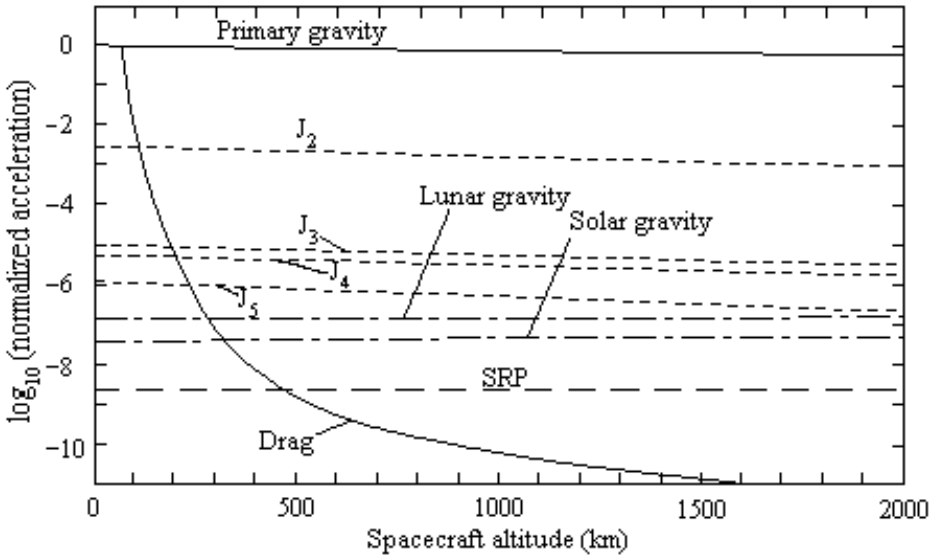

Figure 2.2: Normalised perturbative acceleration as function of the spacecraft altitude [35]

2.4 Lagrange's planetary equations

It is often convenient to represent the motion of the spacecraft through the orbital elements. For a perturbed motion the rates of change of the six orbital elements are expressed by the Lagrange Planetary Equations (see Vallado [32], Curtis [31], Battin [33] for theoretical derivation).

$$\begin{aligned}
\frac{da}{dt} &= \frac{2}{na}\frac{\partial R}{\partial M} \\
\frac{de}{dt} &= \frac{(1-e^2)^{1/2}}{ena^2}((1-e^2)^{1/2}\frac{\partial R}{\partial M} - \frac{\partial R}{\partial \omega}) \\
\frac{d\Omega}{dt} &= \frac{1}{na^2(1-e^2)^{1/2}\sin i}\frac{\partial R}{\partial i} \\
\frac{di}{dt} &= -\frac{1}{na^2\sin i((1-e^2)^{1/2}}(\frac{\partial R}{\partial \Omega} - \cos i\frac{\partial R}{\partial \omega}) \\
\frac{d\omega}{dt} &= \frac{(1-e^2)^{1/2}}{ena^2}\frac{\partial R}{\partial e} - \frac{\cos i}{na^2(1-e^2)^{1/2}\sin i}\frac{\partial R}{\partial i} \\
\frac{dM}{dt} &= n - \frac{2}{na}\frac{\partial R}{\partial a} - \frac{(1-e^2)}{ena^2}\frac{\partial R}{\partial e}
\end{aligned} \tag{2.10}$$

where M is the mean anomaly, n is the mean motion of the satellite and R is the disturbing function and represents the disturbing part of the potential. The mean motion n is computed as

$$n = \sqrt{\frac{\mu}{a^3}} \tag{2.11}$$

Eqs.(2.10) are valid if only conservative forces are considered. The disturbing function R is composed by the sum of the perturbations related to each perturbing source. In the case of a satellite orbiting around the Earth

$$R = R_{\oplus} + R_{\odot} + R_{\leftmoon} \tag{2.12}$$

where $R_{\oplus}$ is the disturbing potential associated to the asymmetry of the gravity field of the Earth, $R_{\odot}$ is the third body disturbing potential of the Sun and $R_{\leftmoon}$ is the third body disturbing potential of the Moon.

2.5 Gauss' form of the variational equations

When the motion of the satellite is influenced also by non-conservative forces, the rate of change of the orbital elements cannot be computed using Eqs.(2.10). Non-conservative perturbations acting on the motion are the disturbance associated to drag or related to manoeuvres performed through the propulsion system of the satellite.
In case of an impulsive firing the instantaneous variation of the six orbital parameters (a, e, i, Ω, ω, M) is computed through Gauss' form of the variational equation. The impulsive firing is characterised by a velocity variation $\delta\mathbf{v} = [\delta v_t \ \delta v_n \ \delta v_h]$ expressed in the $\hat{\mathbf{t}}, \hat{\mathbf{n}}, \hat{\mathbf{h}}$, velocity reference frame (Colombo [36]).

$$
\begin{aligned}
\delta a &= \frac{2a^2 v_d}{\mu}\delta v_t \\
\delta e &= \frac{1}{v_d}(2(e + \cos\theta\delta v_t - \frac{r_d}{a}\sin\theta\delta v_n) \\
\delta\Omega &= \frac{r_d \sin u}{h \sin i}\delta v_h \\
\delta i &= \frac{r_d \cos u}{h}\delta v_h \\
\delta\omega &= \frac{1}{e v_d}(2\sin\theta\delta v_t + (2e + \frac{r_d}{a}\cos\theta)\delta v_n) - \frac{r_d \sin u \cos i}{h \sin i}\delta v_h \\
\delta M &= -\frac{b}{e a v_d}(2(1 + \frac{e^2 r_d}{p})\sin\theta\delta v_t + \frac{r_d}{a}\cos\theta\delta v_n)
\end{aligned}
\tag{2.13}
$$

where r_d and v_d are the orbital radius and the velocity at the point where the impulsive firing is performed, h is the angular momentum, p is the semi-latus rectum and u is the argument of latitude defined as $u = \omega + \theta$. The values of h, p and b are computed as follows

$$h = |\mathbf{r} \times \mathbf{v}| \tag{2.14}$$

$$p = a(1 - e^2) \tag{2.15}$$

$$b = a\sqrt{1 - e^2} \tag{2.16}$$

The Gauss' form of the variational equation reported above are used in this work to compute the effects of the disposal manoeuvre on the orbital elements of the spacecraft. Assuming that the manoeuvres can be approximated with an instantaneous velocity variation whose components are expressed in the $\hat{\mathbf{t}}, \hat{\mathbf{n}}, \hat{\mathbf{h}}$, velocity reference frame, the impulsive variation of the orbital elements is straightforward evaluated using Eqs.(2.13).

2.6 Perturbations

In the present chapter, the expressions of the disturbing potential related to the planet gravitational field and to the presence of a third body are recovered. In case that the effect of the perturbations is conservative, it can be described through a disturbing potential R, containing the effects of the Earth gravity and the third body effects of the Sun and the Moon.

$$R = R_{\oplus} + R_{\odot} + R_{\leftmoon} \tag{2.17}$$

The rate of change of the orbital elements is described by Lagrange's Planetary Eqs.(2.10) which general form can be written as

$$\frac{d\boldsymbol{\alpha}}{dt} = f(\boldsymbol{\alpha}, \frac{\partial R}{\partial \boldsymbol{\alpha}}) \tag{2.18}$$

where $\boldsymbol{\alpha} = [a\ e\ i\ \Omega\ \omega\ M]$. Under the assumption that the six orbital elements are constant over one orbit revolution of the spacecraft around the main attractor, the potential can be replaced by a orbit-averaged form and the variation of the orbital elements is so described as [13] [12]

$$\frac{d\bar{\boldsymbol{\alpha}}}{dt} = f(\bar{\boldsymbol{\alpha}}, \frac{\partial \bar{R}}{\partial \boldsymbol{\alpha}}) \tag{2.19}$$

where $\bar{\alpha}$ is the vector containing the mean orbital elements and $\bar{R}$ is the orbit-averaged disturbing function.

2.6.1 Earth gravity field

The rotational rate of the Earth is responsible of a poles flattening of the planet. This causes the equatorial radius to be 21 km larger than the polar radius [31]. The lacking of symmetry of the Earth's geometry is the cause of the displacement of the gravity vector acting on the satellite from the direction of the center of the main attractor.

For HEO orbit the effect of the Earth's gravitational field is not the principal one. In this thesis, focusing on the disposal of INTEGRAL, only the J_2 term, which denotes the second zonal harmonic coefficient, is considered. In this case the potential for the perturbing effects of a non-spherical central body is expressed by J_2. The averaged potential related the Earth's gravity is [37] [13]

$$\bar{R}_{J_2} = W\frac{na^2}{6}\frac{3\cos^2 i - 1}{(1-e^2)^{3/2}} \tag{2.20}$$

where

$$W = \frac{3}{2}J_2\frac{R_\oplus^2}{a^2}n \tag{2.21}$$

In the equation reported above $J_2 = 1.083 \times 10^{-3}$ represents the second zonal harmonic coefficient and $R_\oplus$ is the mean radius of the Earth.

2.6.2 Third-body perturbation

The three-body system consists of an inner binary system, composed by the main attractor (Earth) and the orbiting body (the satellite), and an outer perturbing body. In this case the outer perturbing body are either the Moon or the Sun. The effects related to the presence of the third body are defined following the approach presented in Kaufman [10]. The disturbing potential due to the third body is

$$R_{3B}(r, r') = \mu'\Big(\frac{1}{|\mathbf{r} - \mathbf{r'}|} - \frac{\mathbf{r}\cdot\mathbf{r'}}{r'^3}\Big) \tag{2.22}$$

where μ' is the gravitational planetary constant of the third body, $\mathbf{r}$

is the position vector of the satellite and **r'** is the position vector of the third body in the inertial reference frame fixed on the main attractor (Earth).
The method defined by Kaufman is based on the expression of the disturbing potential as function of the orbital elements of the satellite, the orientation of the eccentricity and the semi-latus rectum vectors of the satellite with respect to the position of the third body (A, B, their expressions are reported below) and the ratio δ between the semi-major axis of the orbit of the satellite and the magnitude of the position vector of the third body. The expressions of δ, A and B are obtained as follows [12]

$$\delta = \frac{a}{r'} \tag{2.23}$$

$$A = \hat{\mathbf{P}} \cdot \hat{\mathbf{r}}' \tag{2.24}$$

$$B = \hat{\mathbf{Q}} \cdot \hat{\mathbf{r}}' \tag{2.25}$$

where $\hat{\mathbf{P}}$ and $\hat{\mathbf{Q}}$ are respectively the eccentricity unity vector and the semi-latus rectum unit vector of the satellite. Both unit vectors are expressed in the equatorial inertial reference frame.
$\hat{\mathbf{P}}$ and $\hat{\mathbf{Q}}$ are computed through a composition of rotations [12]

$$\begin{aligned} \hat{\mathbf{P}} &= R_3(\Omega)R_1(i)R_3(\omega) \cdot [1\,0\,0]' \\ \hat{\mathbf{Q}} &= R_3(\Omega)R_1(i)R_3(\omega + \frac{\pi}{2}) \cdot [1\,0\,0]' \\ \hat{\mathbf{r}}' &= R_3(\Omega')R_1(i')R_3(u') \cdot [1\,0\,0]' \end{aligned} \tag{2.26}$$

where $u' = \omega' + \theta'$.

A and B can be expressed as function of the orbital elements of the satellite and the variables Ω', ω', i' and θ' which are respectively the RAAN, the anomaly of the perigee, the inclination and the true anomaly of the perturbing third body on its orbit.
In Eqs.(2.26) R_1 and R_3 are rotation matrices that rotate a vector about the origin for a generic angle θ. The rotation matrices are defined as

$$R_1(\theta) = \begin{bmatrix} 1 & 0 & 0 \\ 0 & \cos\theta & -\sin\theta \\ 0 & \sin\theta & \cos\theta \end{bmatrix} \tag{2.27}$$

$$R_3(\theta) = \begin{bmatrix} \cos\theta & -\sin\theta & 0 \\ \sin\theta & \cos\theta & 0 \\ 0 & 0 & 1 \end{bmatrix} \tag{2.28}$$

Under the assumption that δ is small, Eq.(2.22) can be written as a Taylor series in δ [12]

$$R_{3B}(r, r') = \frac{\mu'}{r'} \sum_{k=2}^{\infty} \delta^k F_k(A, E, e, E) \tag{2.29}$$

where the expressions of the coefficients F_k are reported in Kaufman and Dasenbrock [10]. An averaged dynamical model, developed according to the assumptions made in Section 2.6 is implemented in the *PlanODyn* suite [20].

Chapter 3

Atmospheric interface

Skipping stones on the calm surface of a lake is a age-old game. Everyone knows that the perfect throw of a flat shaped stone is a skillfull task. From the experience we learned that only for a strike with the proper velocity and the correct angle of impact on the water the stone will bounce several times before sinking in the water.
The re-entry of a spacecraft in the Earth's atmosphere faces the same challenges. If the impact on the atmosphere is too fast or too sharp the vehicle will experience excessive mechanical and thermal loads. On the other side for a shallow atmospheric entry the spacecraft could bounce on the atmosphere back to the space like a skipping stone.
The first real examples of atmospheric entry were provided by ballistic-missiles developed during the II World War. Later on the re-entry was studied to develop planetary probes for the exploration of the solar system. Typical examples of returns to the atmosphere are the Space Shuttle's returns and the re-entry of the Apollo capsule [1].
Particular constraints are required by manned missions and Sample Return Vehicles (SRV) which, in order to guarantee the survival of the crew, have important constraints on the maximum deceleration and on the temperature that can be reached during the re-entry phase. In this cases special importance is assumed by the maximum heat flux,

the total heat load and the maximum acceleration experienced by the spacecraft during the re-entry phase.
Nowadays, due to the high number of launches of space systems into orbit per year, the density of space debris present in the orbital environment of the Earth is rapidly increasing implying a rise of the probability of catastrophic collisions. For this reason different post-mission disposal guidelines have been introduced in order to keep the space debris environment at a safe level [38]. According to ESA's space debris mitigation guidelines [15] the main requirements introduced to reduce the space debris growth imply a passivation of the spacecraft at the end of the operational life, in order to avoid accidental explosions in orbit, and the design of collisions avoidance manoeuvres while the spacecraft is still operative to reduce the risk of on-orbit collisions. In order to prevent an uncontrolled passage of the spacecraft in orbital protected regions after the end of the mission of the spacecraft, post mission guidelines require the design of a proper disposal strategy that will bring the spacecraft into a 'graveyard orbit' or that will lead to a safe atmospheric entry within 25 years. In this context, during the design of a strategy that will lead the satellite to an atmospheric re-entry, it is fundamental to produce a prediction of the behaviour of the space system during the destructive phase. For this reason the theoretical concept of overshoot boundary is introduced in the following Section, with the intent to exploit the method as effective interface between the long-term propagation and the destructive re-entry phases.

3.1 Overshoot boundary

When the satellite begins the atmospheric entry the orbit is completely characterised, within the plane of motion, given the flight–path angle γ_1, the velocity v_1 and the radius r_1 (see Figure 3.1). The condition at the entry interface are γ_e, v_e and r_e. If the conditions at a generic point 1 are known, then the entry condition, once the altitude of the

atmospheric interface r_e is defined, can be computed. As derived in Hicks [1] the velocity at the atmospheric entry can be computed as

$$V_e = \sqrt{\mu\left(\frac{2}{r_e} - \frac{1}{a}\right)} \tag{3.1}$$

The flight-path angle can be computed considering that the specific momentum is conserved

$$h = r_1 V_1 \cos\gamma_1 = r_e V_e \cos\gamma_e \tag{3.2}$$

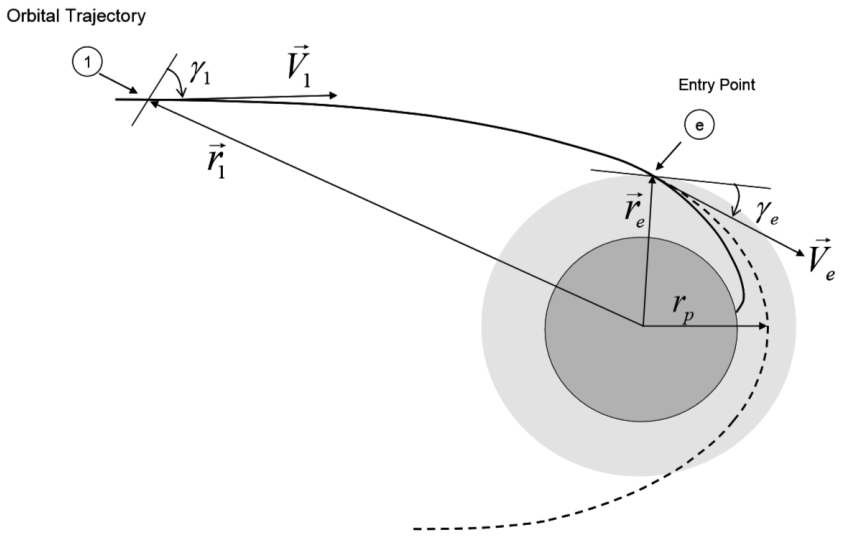

Figure 3.1: Atmospheric Entry Conditions [1]

For different trajectories the vehicle can behave in different ways. If the entry angle is too shallow, the vehicle may pass through the upper layer of the atmosphere and continue is path in the space environment. On the other side if the entry angle is too steep at the

entry interface, the spacecraft will be affected by high mechanical and thermal loads that could exceed the maximum loads allowed by the mission requirements. All the trajectories between these two extreme situations ensure not only that the spacecraft will be captured during its atmospheric passage, but also that the re-entry conditions will not exceed the design limits.
Figure 3.2 shows the two boundaries that characterise the atmospheric entry of the satellite. The overshoot boundary is defined by the maximum periapsis radius $r_{p_{overshoot}}$ which allows the satellite to achieve re-entry conditions at the first atmospheric passage. Above the overshoot boundary the satellite encounters too small atmospheric drag and will not be captured.
If the mission design includes requirements on the loads that the vehicle can withstand during the re-entry phase, i.e. manned missions or SRVs, the definition of an undershoot boundary becomes of primary importance. The undershoot boundary $r_{p_{undershoot}}$ is in fact related to the maximum deceleration allowed along the re-entry trajectory. If the the vehicle enters the atmosphere below this limit it will experience too much drag: the undershoot boundary is therefore a representation of the border between "safe" and "unsafe" entry.
The entry corridor is straightforward defined by the difference

$$\Delta r_p = r_{p_{overshoot}} - r_{p_{undershoot}} \tag{3.3}$$

In the case which the concept of entry corridor is used for the analysis of the atmospheric entry of a satellite at end-of-life, there are no constraints on the maximum deceleration and heat loads that the vehicle shall face. For this reason the only significant condition is related to the expression of the overshoot boundary.

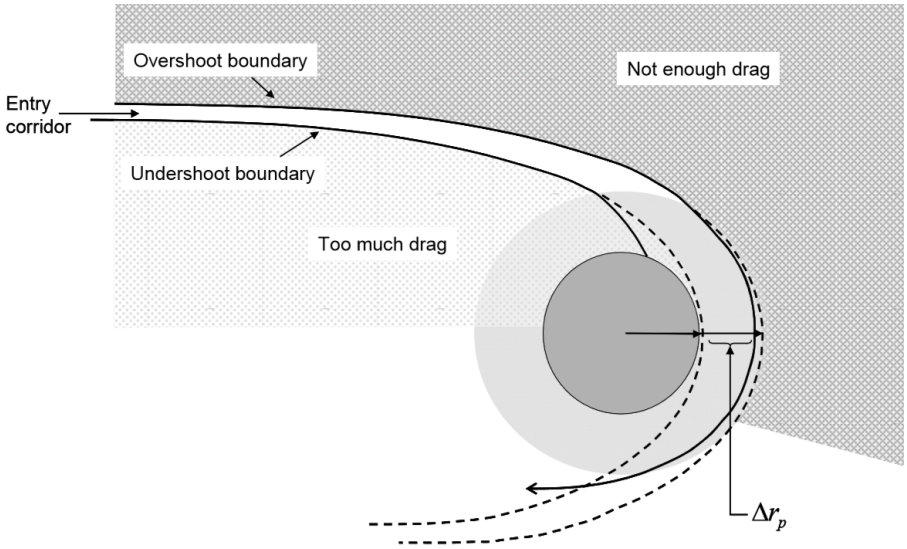

Figure 3.2: Entry Corridor [1]

3.2 Unified theory

The unified theory presented in this section follows the approach adopted in Hicks [1], obtained following the method described by Vinh [39]. The main issues that affect the analysis of a re-entry strategy are related to the impossibility of defining an exact border between the deep space and the Earth's atmosphere and to the difficulty of identifying the flight conditions that will allow an atmospheric capture of the spacecraft.
The approach based on the overshoot theory presented below provides a tool for the re-entry prediction based on the deceleration experienced by the satellite along its trajectory. The approach solves therefore the problem of predicting the conditions that will lead the vehicle to achieve a re-entry at the first atmospheric passage without assuming a fixed altitude for the atmospheric interface.
To compute the overshoot boundary we have to select an arbitrary value f for the ratio between the deceleration and the gravity acceleration. We assume that when the ratio a_{decel}/g_o reaches the value f then the atmospheric entry occurs. Along the overshoot boundary the ratio defined above should therefore never drop below f. The value of f is somewhat arbitrary. In this work we will follow Vinh's indication and set it equal to 0.05.
The atmospheric density used is approximated with a strictly exponential model:

$$\rho(r) = \rho_0 e^{-\beta r} \tag{3.4}$$

where β is the inverse of atmospheric scale height and ρ_0 is the atmospheric density at the planet surface. For the case in exam $\rho_0 = 1.225\ kg\,m^{-3}$, which is the standard atmospheric value at sea-level. The theory presented in this section follows Vinh's theory and is based on the definition of two adimensional variables called "modified" Chap-

man variables

$$F = \frac{\rho(r) S C_D}{2m} \sqrt{\frac{r}{\beta}} = Z \tag{3.5}$$

$$u = \frac{v^2 \cos^2 \gamma}{g(r) r} \tag{3.6}$$

where ρ is the atmospheric density at distance r. S is the cross-sectional area of the spacecraft, C_D is the drag coefficient, m is the mass of the vehicle, β is again the inverse of the atmospheric scale height, g is the gravitational acceleration and v and γ are respectively the velocity and the flight path angle of the vehicle.
The gravity term in the equations defined above is defined with an inverse square central gravity term

$$g(r) = \frac{\mu}{r^2} \tag{3.7}$$

The procedure to build the overshoot boundary is obtained as follows (see Hicks [1] for theoretical reference).

- **STEP 1:** Choose a value for Z_*. The value defines the point of critical deceleration, where $(a/g_0) = f$.

- **STEP 2:** Solve

$$2\sqrt{\bar{\beta} r} Z_* + (\bar{\beta} r - 1) \sin \gamma_* + \frac{2 \sin \gamma_* \cos^2 \gamma_*}{u_*} = 0 \tag{3.8}$$

  and

$$\left(\frac{a_{decel}}{g_0}\right)_* = \frac{Z_* u_* \sqrt{\bar{\beta} r}}{\cos^2 \gamma_*} + \sqrt{1 + \left(\frac{C_L}{C_D}\right)^2} = f \tag{3.9}$$

for the adimensional kinetic energy u_* and the flight-path angle γ_*, where C_L is the lift coefficient of the spacecraft and $\bar{\beta r}$ is an average value characterising the atmosphere considered. The solution defined by Z_*, u_* and γ_* represents a point of minimum deceleration on the trajectory.

- **STEP 3:** Recover the entry conditions Z_e, u_e and γ_e.

$$\frac{dZ}{ds} = -\bar{\beta r} Z \tan\gamma \tag{3.10}$$

$$\frac{du}{ds} = \frac{2Zu\sqrt{\bar{\beta r}}}{\cos\gamma}\left(1 + \frac{C_L}{C_D}\cos\sigma\tan\gamma + \frac{\sin\gamma}{2Z\bar{\beta r}}\right) \tag{3.11}$$

$$\frac{d\gamma}{ds} = \frac{Z\sqrt{\bar{\beta r}}}{\cos^2\gamma}\left[\frac{C_L}{C_D}\cos\sigma + \frac{\cos\gamma}{Z\bar{\beta r}}\left(1 - \frac{\cos^2\gamma}{u}\right)\right] \tag{3.12}$$

The equations are expressed using the arc-length s traveled by the spacecraft. The entry conditions are calculated integrating Eqs. (3.10), (3.11) and (3.12) "backwards" along s until the condition $(a_{decel}/g_0) = f$ is obtained again. The variable σ represents bank angle, which is kept constant during the motion of the spacecraft. The equations reported above represent a two-point boundary value problem. The boundary conditions are defined as

$$Z = Z_*, u = u_*, \gamma = \gamma_* \tag{3.13}$$

at $s = s_*$, and

$$\frac{Z_e u_e \sqrt{\bar{\beta r}}}{\cos^2\gamma_e} + \sqrt{1 + \left(\frac{C_L}{C_D}\right)^2} = f \tag{3.14}$$

at $s = 0$

- **STEP 4:** Solve equation

$$\frac{u_e^2}{\cos \gamma_e{}^2} - 2u_e = u_p^2 - 2u_p \tag{3.15}$$

and

$$Z_p = Z_e \sqrt{\frac{u_e}{u_p}} exp\left[\bar{\beta r}\left(1 - \frac{u_e}{u_p}\right)\right] \tag{3.16}$$

simultaneously to find $F_{p_{over}} = Z_{p_{over}}$

Repeating the procedure presented above for different values of Z_* allows us to obtain the expression of the periapsis parameter Z_p as a function of the velocity ratio defined as

$$\frac{v_e}{v_c} = \sqrt{\frac{u_e}{\cos^2 \gamma_e}} \tag{3.17}$$

where v_e is the entry speed and v_c is the circular speed.
Once the atmosphere has been specified with a characteristic average $\bar{\beta r}$, the procedure above can be performed for each set of specified entry conditions, constant lift-to-drag ratio C_L/C_D and constant bank angle σ. For the case in exam $(C_L/C_D) = 0$, in agreement to the assumption of random motion for the entry of uncontrolled satellites. For Earth's atmosphere the average value $\bar{\beta r}$ is set equal to 900 [1].
The overshoot boundary represented in Figure 3.3 is obtained by varying Z_* in a range between 1.68×10^{-3} and 1.91×10^{-3}, according to the indication presented in Hicks [1].
This approach allows us to study the atmospheric entry of a space system without requiring detailed information about the vehicle before beginning the analysis. For this reason the overshoot boundary, which

can be pre-computed without using any information about the satellite configuration, is a helpful tool to estimate when the evolution of the orbital elements reaches conditions that can lead to an atmospheric re-entry. The expression of the overshoot boundary is based on adimensional variables and once the parameters that influence the boundary (C_L/C_D, $\bar{\beta r}$) are defined for the mission in exam, the computation of the overshoot boundary is straightforward. The overshoot boundary can therefore be pre-computed and applied for the re-entry prediction in missions characterised by the same parameters.

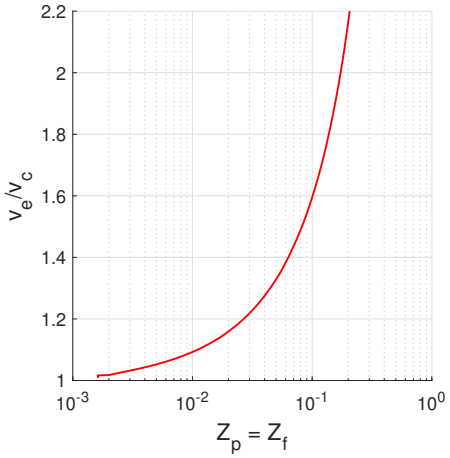

Figure 3.3: Overshoot Boundary computed for Ballistic Entry ($C_L/C_D = 0$ into Earth's atmosphere ($\bar{\beta r} = 900$). The result is obtained considering a deceleration ratio $f = 0.05$.

Chapter 4

INTEGRAL Re-entry prediction

4.1 Mission overview

On 17 October 2002 a Russian Proton launcher successfully placed ESA's International Gamma-Ray Astrophysics Laboratory INTEGRAL into orbit. The task of INTEGRAL, the most sensitive gamma-ray observatory ever launched, is to gather some of the most energetic radiation coming from space, performing fine spectroscopy and fine imaging of gamma-rays emitted by celestial sources while monitoring the sources in the X-ray and optical energy ranges [40].
The Earth's atmosphere does not allow the passage of these high energy radiations. For this reason INTEGRAL is placed in a Highly Elliptic Orbit, so that the satellite can spend most of the time outside the Earth's radiation belts and avoid interference radiation.
The spacecraft is composed by a service module in the lower part, that provides the housekeeping equipment, and a payload module, that carries the scientific instruments (Figure 4.1). The scientific instruments contained in the satellite have a total mass of around 2000 kg, making this payload the heaviest payload ever placed in orbit by ESA. The total mass of the satellite is of more than 4000 kg. Due to the dimensions of the satellite, an estimation of the destructive uncontrolled re-entry

is necessary to check the on-ground risks associated to the disposal manoeuvre.

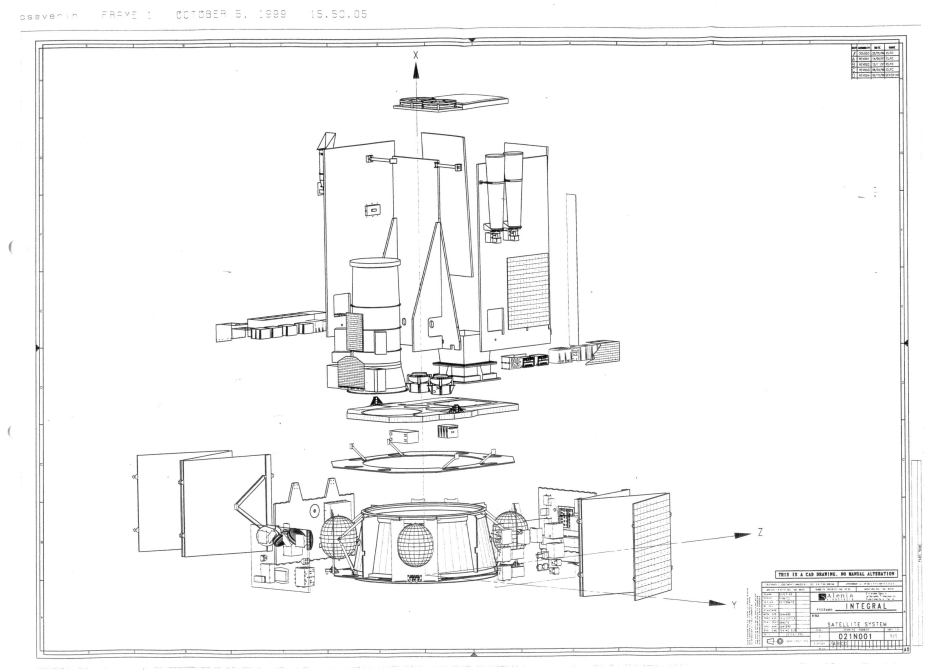

Figure 4.1: Exploded diagram of the INTEGRAL spacecraft. Payload module (upper part) and service module (lower part) [2].

4.2 Disposal strategy

In the present section the unified theory presented is used to analyse the disposal trajectory of INTEGRAL. The disposal strategy considered was obtained by Colombo et al. [11] through an optimisation procedure. The re-entry of the satellite is obtained with a single-manoeuvre that modifies the orbital parameters allowing the satellite, affected by luni-solar perturbations, to a long-term uncontrolled re-entry.
The orbital dynamics of the spacecraft was propagated using *PlanODyn* [13], starting from 2002/11/13 at 00:00 with initial keplerian elements as reported in Table 4.1. All the orbit propagations are performed considering the luni-solar perturbation and the effect of non-spherical gravity field.

Parameter	**Value**
a	87736 km
e	0.82403 [-]
i	0.91939 rad
Ω	1.7843 rad
ω	5.271 rad
M	1.4439 rad

Table 4.1: Orbital Elements on 2002/11/13 at 00:00.

The manoeuvre is completely characterised with four parameters that describe the magnitude, the position, and the direction of the impulsive velocity variation that is applied to the spacecraft. The instantaneous variation of the six orbital elements can so be expressed as

$$\delta\alpha = \delta\alpha(\Delta v, \alpha, \beta, \theta) \tag{4.1}$$

where α and β are respectively the in-plane an the out-of plane

angles expressed in the $\hat{\mathbf{t}}, \hat{\mathbf{n}}, \hat{\mathbf{h}}$, reference frame, Δv is the magnitude of the velocity change and θ is the true anomaly at the point where the manoeuvre is performed.
The impulsive velocity change characterised by a magnitude Δv is modeled as

$$\Delta \mathbf{v} = \Delta v \begin{bmatrix} \cos\alpha \cos\beta \\ \sin\alpha \cos\beta \\ \sin\beta \end{bmatrix} \tag{4.2}$$

The focus is on the manoeuvre n.5 [11]. The manoeuvre considered is characterised by impulsive velocity change performed on 08/08/2014 at 9:00 A.M.. The parameters that fully describe the disposal manoeuvre are reported in Table 4.2.

Parameter	**Value**
Δv	26.26 m/s
α	173.4 deg
β	35.4 deg
θ	45.1 deg

Table 4.2: Magnitude, in- and out-of plane angles and true anomaly of the disposal strategy corresponding to manoeuvre n.5.

The variation of the orbital elements due to the impulsive manoeuvre is computed through Gauss' Form of the Variational Equations. The new orbital elements are then used to propagate the orbital dynamics until a perigee altitude of 50 km is achieved. The evolution of the perigee altitude and of the orbital elements of the satellite over 30 years is shown in Figure 4.2 and 4.3, in accordance with the results reported in Colombo et al. [11] .

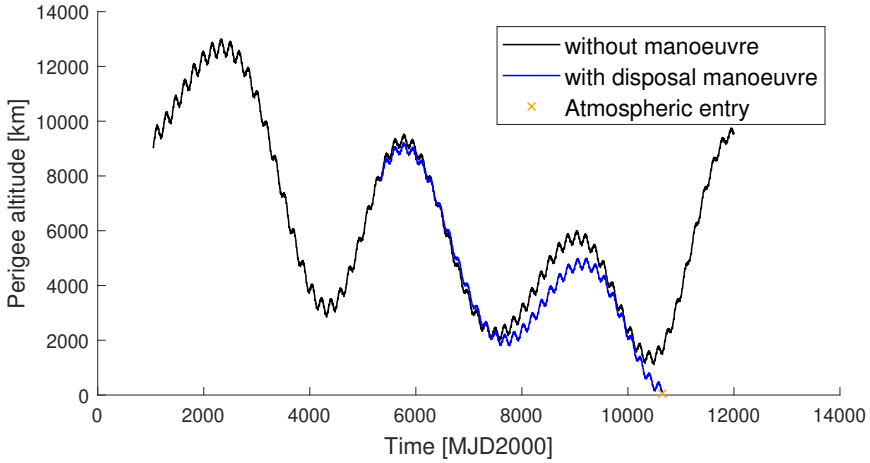

Figure 4.2: Perigee altitude evolution of INTEGRAL. The black line depicts the natural perigee evolution over 30 years. The blue line shows how the long-term evolution after the disposal manoeuvre leads to the atmospheric entry of INTEGRAL.

The entry conditions are then recovered considering a fixed altitude for the atmospheric interface of 120 km. Following the procedure reported above the entry velocity obtained is equal to 10.86 km/s, much higher than the typical re-entry velocity from LEO according to the consideration that the re-entry conditions are achieved without a circularisation of the orbit.

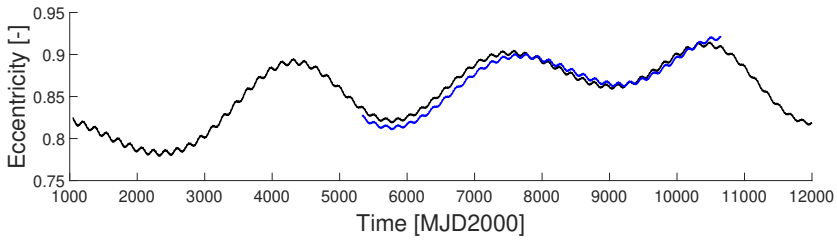

(a)

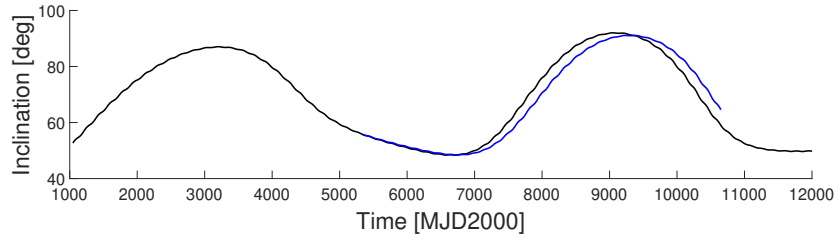

(b)

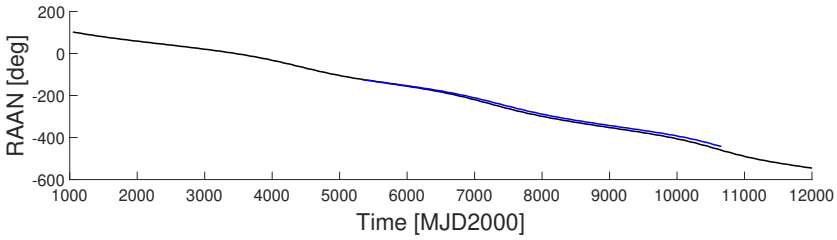

(c)

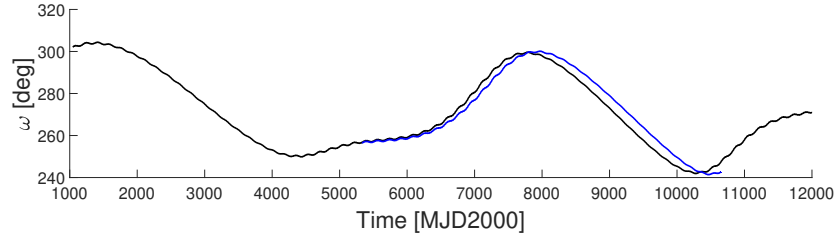

(d)

Figure 4.3: Orbital elements evolution. Natural evolution of INTEGRAL (black line) and disposal strategy (blue line).

4.3 Re-entry estimation exploiting the overshoot boundary theory

In previous works the re-entry prediction of INTEGRAL was performed assuming a target altitude of 50 km and a fixed altitude for the atmospheric interface, neglecting therefore the contribution of the atmospheric drag [11]. The overshoot boundary theory provides a method that allows us to take into account these effects in the re-entry prediction. The prediction of the conditions that can lead to an atmospheric capture are so computed considering the effect of drag, that assumes primary importance at low altitudes.
this section reports the re-entry estimation obtained exploiting the overshoot boundary theory relative to the disposal strategy of INTEGRAL defined above.

4.3.1 Characteristics of INTEGRAL

The re-entry prediction is performed for an area-to-mass ratio associated to an average value for the cross-section according to the assumption of random tumbling of the spacecraft. The average cross-section is computed as

$$S = \frac{1}{3}(A_{SP} + WH + LH + LW) \tag{4.3}$$

where A_{SP} is the solar panels area and W, H and L are the dimensions of INTEGRAL in the orbit configuration as defined in Table 4.3. Figure 4.4 shows the configuration of INTEGRAL in orbit.

Dimension	**Value**
Solar Panels Area	21.9 m^2
L	2.175 m
W	3.138 m
H	4.939 m
Dry mass	3414 kg

Table 4.3: Characteristics of INTEGRAL's configuration on orbit.

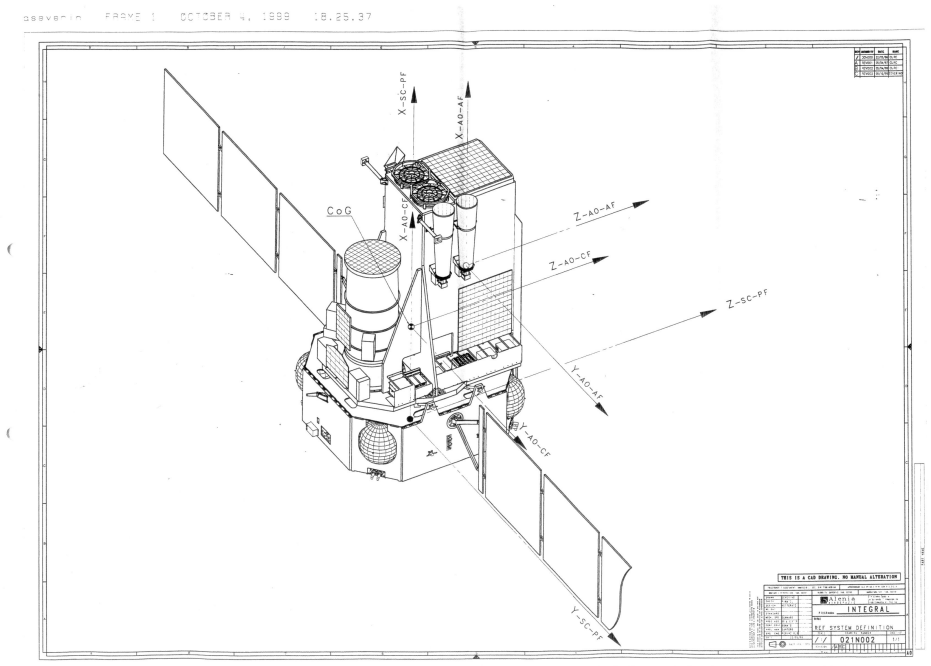

Figure 4.4: INTEGRAL: Satellite Configuration in Orbit [41].

4.3.2 Drag coefficient

During the atmospheric re-entry, the spacecraft encounters different flow conditions, passing from free-molecular to continuum regime. The drag coefficient is therefore not constant. The expression of the drag coefficient as function of the Knudsen number for free-molecular and continuum flow are recovered from Klett [42] and a bridging function

is used to connect the flow conditions mentioned above [43]. The expressions provide an estimation of the drag coefficients for cylinders in free-molecular and continuum flow for hypersonic flight conditions. Following the approach adopted in previous works the expressions have been adapted for a box structure to obtain an estimation of the trend of the drag coefficient [30].

$$C_{D_{fm}} = 1.57 + 0.785\frac{W}{L} \tag{4.4}$$

$$C_{D_c} = 1.83(0.393 + 1.178\frac{W}{L}) \tag{4.5}$$

$$C_{D_t}(Kn) = C_{D_c} + (C_{D_{fm}} - C_{D_c})(\sin(\pi(0.5 + 0.25log_{10}Kn)))^3 \tag{4.6}$$

The equations reported above express the variation of the drag coefficient at different altitudes. Eq.(4.4) is valid for Kn>1, Eq.(4.5) for Kn<0.01 and Eq.(4.6) expresses the coefficient trend in the transition regime. Figure 4.5 reports the trend of C_D in the transition regime for different geometries of the spacecraft. It can be noted that the expressions reported above are highly influenced from the ratio W/L.
For the re-entry estimation performed in this work a constant drag coefficient has been assumed. The drag coefficient was selected computing the average value of the coefficient along the Knudsen number, considering the different geometries that could be used to describe the configuration of INTEGRAL using a simplified cylindrical shape. All the computations performed in this work assume a constant drag coefficient $C_D = 2.2$. The selected value is in accordance with the drag coefficient assumed for INTEGRAL in other works [11] [21].

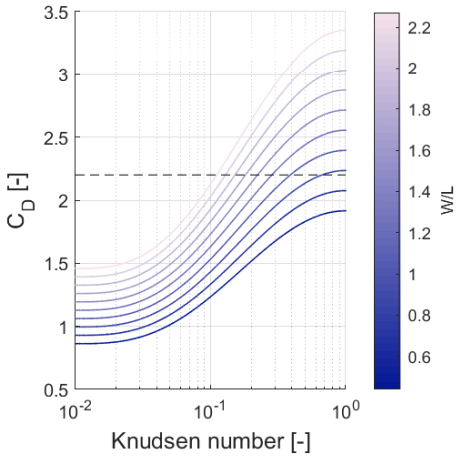

Figure 4.5: Drag coefficient function of the Knudsen number in the transition regime. The continuous line depicts the trend of the drag coefficient for different geometries of the spacecraft. The dotted line represents the constant approximation adopted for the expression of the coefficient.

4.3.3 Methodology

The theory presented in Section 3.2 is used to estimate the conditions on the orbital parameters that correspond to an atmospheric re-entry. The overshoot boundary is used to estimate the time instant when the entry conditions are reached.

Once the parameters that influence the boundary are defined (C_L, C_D and $\bar{\beta r}$), the computation of the overshoot boundary can be performed as presented in Section 3.2. During the procedure, for each value of Z_p the associated values of Z_e and u_e are obtained. Recall that Z_e and u_e are the adimensional Champan's variables at the entry interface and can be associated to the entry altitude and velocity.

Note that, considering that the expression of the overshoot boundary is based on adimensional variables, the boundary can be precomputed and can be used for the re-entry prediction of different missions characterised by the same average atmosphere property ($\bar{\beta r}$) and the same lift-to-drag ratio (C_L/C_D).

The computed values are used to obtain an explicit expression of the variables at the entry interface as function of Z_p.

$$Z_e = Z_e(Z_p) \tag{4.7}$$

$$u_e = u_e(Z_p) \tag{4.8}$$

the expressions represented by Eqs.(4.7) and (4.8) are obtained through a polynomial interpolation of the set of data obtained during the computation of the overshoot boundary and allow the re-entry prediction of different missions.
At each time step the following procedure must be performed to check if the re-entry conditions are met.

- **STEP 1:** The value of Z_{p_d} of the disposal orbit must be computed solving Eq.(3.5).

- **STEP 2:** From Z_{p_d} the respective values of Z_e and u_e are recovered through Eqs.(4.7) and (4.8).

- **STEP 3:** Compute the radius at the entry interface r_e solving Eq.(3.5) for the value of Z_e recovered in the previous step.

- **STEP 4:** Find the true anomaly at the entry interface as

$$\theta_{entry} = \arccos\left(\left(\frac{1}{e}\right)\left(\left(\frac{e}{r_e}\right)(1-e^2)-1\right)\right) \tag{4.9}$$

- **STEP 5:** Find the velocity v_{e_d} and the flight-path angle γ_{e_d} of the disposal at the overshoot boundary

$$v_{e_d} = \sqrt{\mu\left(\frac{2}{r_e} - \frac{1}{a_d}\right)} \tag{4.10}$$

$$\gamma_{e_d} = \arctan\left(\frac{e \sin\theta_{entry}}{1 + e\cos\theta_{entry}}\right) \tag{4.11}$$

- **STEP 6:** Compute the adimensional entry velocity u_{e_d} using v_{e_d} and γ_{e_d} in Eq.(3.6).

$$u_{e_d} = \frac{{v_{e_d}}^2 \cos^2\gamma_{e_d}}{gr} \tag{4.12}$$

- **STEP 7:** If $u_{e_d} < u_{e_b}$ the orbit meets the conditions that can lead to an atmospheric entry.

Note that even if the orbit meets the conditions that can lead the spacecraft to an atmospheric entry, it must be checked that the real position of the spacecraft is nearby the overshoot interface. The check can be performed comparing the current mean anomaly of the spacecraft obtained from the long-term propagation and the mean anomaly corresponding to θ_{entry}.

4.3.4 Entry estimation

The trend of the adimensional Champan's variables Z_{p_d} and u_{e_d} for the disposal trajectory of INTEGRAL obtained using manoeuvre n.5 is reported in Figure 4.6. The blue cross represents the first point where the adimensionalised velocity at the entry interface drops below the conditions that define the overshoot boundary. Note that even if

the conditions to obtain an atmospheric entry are reached, the first point where the re-entry actually occurs is when the condition

$$M = M_{entry} \tag{4.13}$$

is verified. In Eq.(4.13) M represents the mean anomaly of the orbit obtained through the long-term propagator and M_{entry} represents the mean anomaly associated to the true anomaly θ_{entry} at the entry interface computed using the unified overshoot boundary theory as reported above.

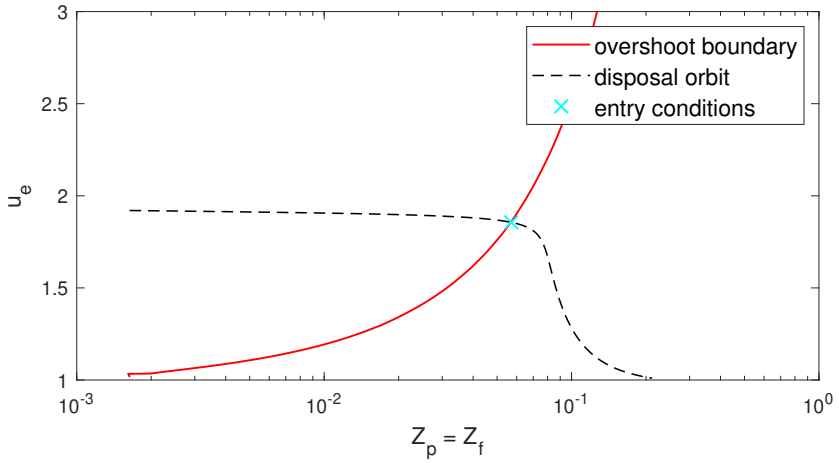

Figure 4.6: Comparison of the final part of the disposal trajectory with the overshoot boundary. The blue cross represents the first time instant when the spacecraft velocity drops below the overshoot boundary.

4.4 Area-to-mass ratio variation

If the satellite is equipped with solar panels, their presence increases the drag acting on the satellite. Due to the increased drag coefficient, the trajectory of the complete space system will be different from the trajectory obtained considering only the main body. Object-oriented models for the analysis of the atmospheric re-entry of a satellite are based on the assumption that the solar panels will usually break-off at an altitude of $\sim$ 95 km [44]. Considering that HEO are characterised by high energetic content the disposal trajectory can therefore present different low altitude passages before the entry conditions are met. Early low altitude passages can be responsible of a break-off of the solar panels, that corresponds to a variation of the area-to-mass ratio of the spacecraft.
This section analyses the effect of selecting different values for the area-to-mass ratio on the re-entry prediction. In particular the re-entry estimation using the unified overshoot boundary theory is performed for two different values of the average cross-section area. The re-entry estimation obtained in the previous section is compared with the re-entry obtained considering only the main body of the spacecraft. The cross-section area is computed according to Eq.(4.3) considering the cross-sectional averaged area without solar panels.

$$S = \frac{1}{3}(WH + LH + LW) \tag{4.14}$$

The values of area-to-mass ratio defining the two conditions are reported in Table 4.4. Note that the area-to-mass ratio after the detachment of the solar panels is computed considering only a variation of the average cross-section area and no mass variation is taken into account. The purpose of the simulation is only to retrieve the qualitative effect of the area-to-mass ratio on the re-entry prediction.

Area-to-mass ratio	Value
with solar panels	0.0054 $[m^2/kg]$
w/o solar panels	0.0032 $[m^2/kg]$

Table 4.4: Area-to-mass ratio values of INTEGRAL

From Figure 4.7 it can be noted, as expected, that for an area-to-mass ratio relative to the presence of the solar panels allows us to reach conditions "below" the overshoot boundary faster that the case computed considering the absence of solar panels. The lower area-to-mass ratio propagation is affected by a higher decrease of the adimensional velocity before the entry conditions are reached. The aerodynamic behaviour of the satellite changes using different approximated models to describe the spacecraft, leading to different re-entry predictions.
In particular this chance is highlighted in Figure 4.8. The figure shows the evolution of the true anomaly of the entry interface in the last part of the trajectory. At each time instant the true anomaly of the entry interface θ_{entry} is computed considering an area to-mass-ratio equal to $(S/m)_{MAX}$ (dashed line) and $(S/m)_{MIN}$ (dotted line). The blue crosses represent the first time instants where the condition $u_{e_d} < u_{e_b}$ is verified in the two cases. It can be noted that this condition is reached before if an higher area-to-mass ratio is considered. The area-to-mass ratio is therefore influencing the entry prediction in two ways. Firstly, a lower cross-section implies lower true anomalies in the overshoot theory predicting generally a later re-entry, in agreement with the consideration that the re-entry prediction is based on the drag effects. On the other side, a higher cross-section will reach the required deceleration at higher altitudes. Secondly, the area-to-mass ratio is influencing the time epoch when we are firstly passing below the overshoot boundary. For this reason, for a lower value of cross-section area, a higher number of low-altitude passages could be performed, leading to a later entry prediction and implying so a higher circularisation of the entry orbit.

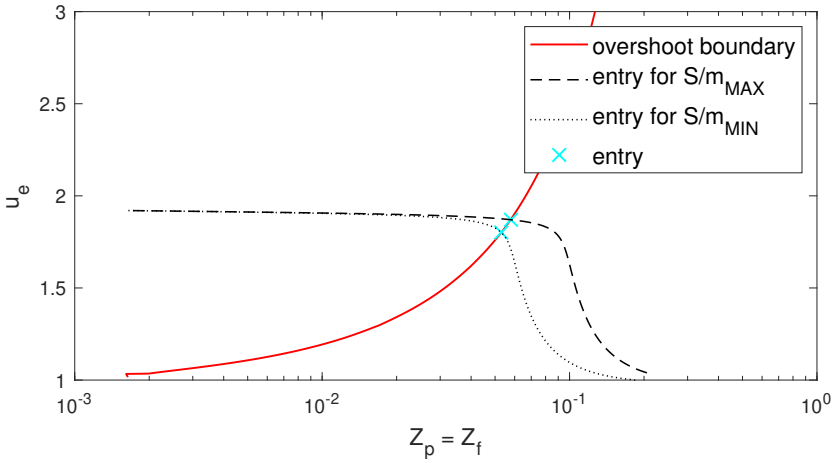

Figure 4.7: Final part of the disposal trajectory. Comparison between the trend of u_e for $(S/m)_{MAX}$ and $(S/m)_{MIN}$ and the overshoot boundary.

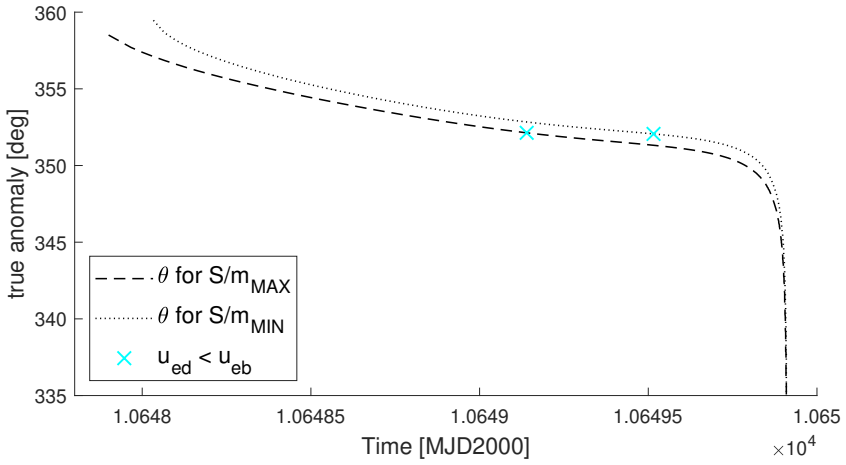

Figure 4.8: True anomaly at entry interface for $(S/m)_{MAX}$ (dashed line) and $(S/m)_{MIN}$ (dotted line).

The orbit characteristics at the time instant when the entry conditions are obtained are summarised in Table 4.5. The first column reports the entry conditions obtained considering a fixed altitude of 120 km for the atmospheric interface. The orbit is propagated until a

perigee altitude of 50 km is reached. Recall that the method adopted does not take into account the effects of atmospheric drag resulting in a highly elliptical entry orbit.
The effects of atmospheric drag are instead taken into account if the overshoot theory is used as interface method. The entry conditions are reported in the second and third column of Table 4.5. The final part of the orbit propagation is highly influenced by atmospheric drag. The re-entry prediction performed with the overshoot theory leads to entry orbits affected by a higher circularisation and is characterised by generally lower eccentricity. The predicted entry orbit without solar panels is characterised by even lower semi-major axis and eccentricity. The difference is produced by the drag effects that are in this case affecting the spacecraft for a longer time resulting in an entry trajectory with even lower flight-path angles.

	fixed interface	**$(S/m)_{MAX}$**	**$(S/m)_{MIN}$**
a	82304.71 [km]	55842.46 [km]	49105. 33 [km]
e	0.9219 [-]	0.8847 [-]	0.8689 [-]
i	64.60 [deg]	64.67 [deg]	64.65 [deg]]
h_{entry}	120 [km]	99.13 [km]	95.48 [km]
v_{entry}	10.86 [km/s]	10.77 [km/s]	10.73 [km/s]
γ_{entry}	-5.84 [deg]	-3.78 [deg]	-3.75 [deg]

Table 4.5: Entry conditions with fixed interface method and overshoot boundary theory for $(S/m)_{MAX}$ and $(S/m)_{MIN}$.

4.5 Uncertainty analysis

The propagation of manoeuvre n.5 is performed taking in account uncertainties for the magnitude of the velocity variation and for the in- and out-of-plane angles. The computation are performed for a set of values setting the nominal manoeuvre as reported in Table 4.2. The error on the magnitude of the velocity vector is introduced according to INTEGRAL's disposal manoeuvre details reported by Merz et al. [23] and summarised in Table 4.6. The disposal strategy is characterised by a composition of four distinct manoeuvres. The uncertainties on the in-plane and out-of plane angles are selected according to the pointing and attitude requirements reported in INTEGRAL manual [45]. The results presented in the next section are obtained considering a normal distribution around the nominal values considering a standard deviation of 2% for the velocity magnitude and of 0.25 degrees for both manoeuvre angles.

Manoeuvre	**1**	**2**	**3**	**4**
Planned Δv	8.393 m/s	14.913 m/s	6.896 m/s	0.146 m/s
Estimated Δv	7.733 m/s	14.964 m/s	6.817 m/s	0.158 m/s
Deviation	+0.660 m/s	-0.051 m/s	+0.079 m/s	-0.012 m/s

Table 4.6: Integral disposal manoeuvre details [23].

4.5.1 Constant area-to-mass ratio

The following results are obtained considering 100 test cases for the re-entry trajectory taking into account manoeuvre uncertainties as reported in Section 4.5. The random set of Δv, α and β values (see Figure 4.9) considered in the test cases are reported in Figure 4.10.

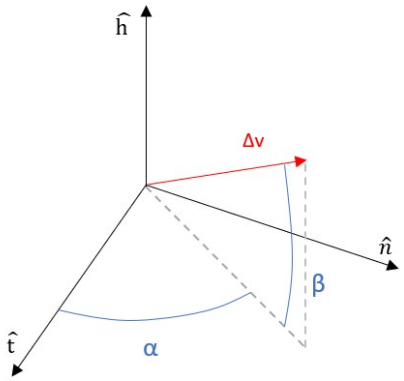

Figure 4.9: Impulsive velocity variation (Δv), in-plane (α) and out-of-plane angles (β)in the $\hat{\mathbf{t}}, \hat{\mathbf{n}}, \hat{\mathbf{h}}$ reference frame.

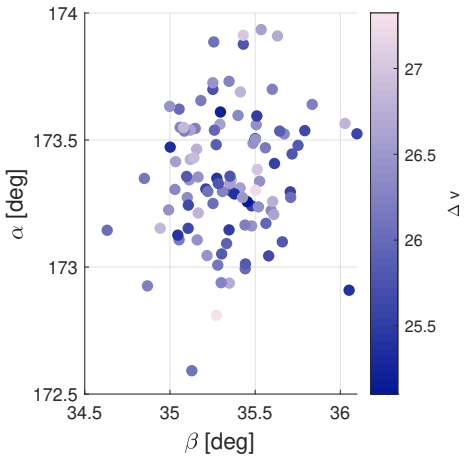

Figure 4.10: Distribution of manoeuvre characteristics affected by uncertainties: 100 test cases.

The propagation of the 100 test cases is firstly performed without the contribution of the atmospheric drag, until a target perigee altitude of 50 km is reached. Figure 4.11 shows the evolution of the perigee altitude of the test cases around the re-entry epoch. It can be noted that the uncertainty on the disposal manoeuvre can produce trajectories

(the 15% of the test cases) that are not reaching the target perigee. Figure 4.12 presents the distribution of the entry conditions computed recovering the conditions of the spacecraft at an altitude of 120 km. The figure highlights the fact that all the trajectories present entry conditions close to the entry conditions that characterise the nominal trajectory (see values in Table 4.5).
The long term propagation and the re-entry prediction using the overshoot theory are then performed considering a constant area-to-mass ratio equal to the initial satellite configuration in orbit ($(S/m)_{MAX}$) and are compared with the results obtained considering an area-to-mass ratio without solar panels ($(S/m)_{MIN}$).

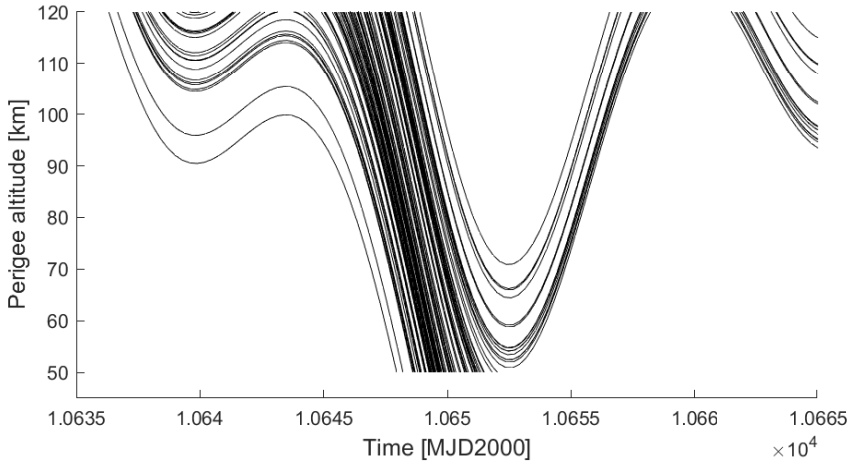

Figure 4.11: Perigee evolution of 100 test cases without drag. Target perigee altitude at 50 km.

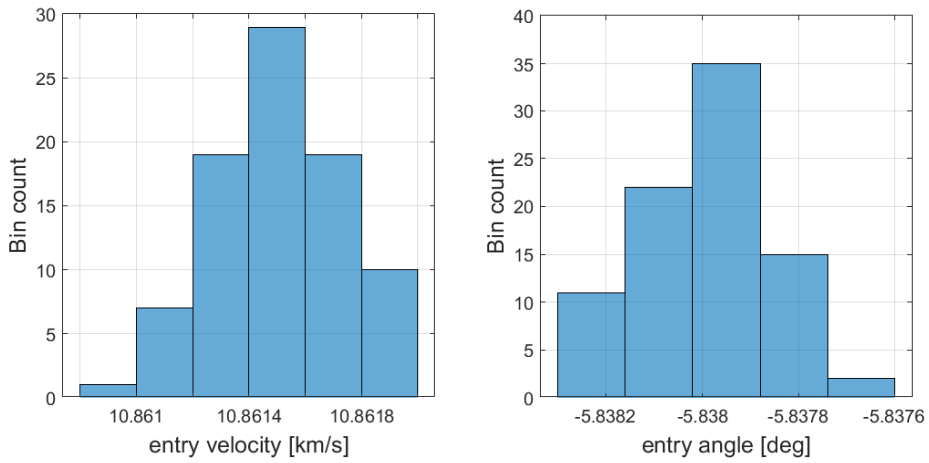

(a) (b)

Figure 4.12: Distribution of the predicted entry velocity (a) and entry angle (b) for 100 test cases. Entry conditions obtained considering a fixed interface at an altitude of 120 km.

Figure 4.13 and 4.14 show the distribution of the entry conditions of the test cases. Some global differences are noticeable between the entry conditions obtained with a fixed interface (Figure 4.12) and the conditions obtained using the overshoot theory (Figure 4.13). If the drag effect is taken into account the 98% of the entry trajectories is characterised by a entry velocity between 9.8 and 10.8 km/s. The 96% of the trajectories have and entry flight-path angle between -3.4 and -3.9 degrees. The smaller entry angles with respect to the conditions obtained considering a fixed atmospheric interface are justified considering the approach adopted to perform the re-entry prediction. The unified theory predicts the spacecraft to achieve re-entry conditions when a certain ratio between the drag deceleration and the gravity acceleration is reached. The deceleration necessary is reached at low true anomalies, close to the pericentre of the orbit. In the final part of the orbit the atmospheric drag effect, that is not considered with a fixed interface approach, reduces the eccentricity of the orbit, implying

re-entry trajectories with lower entry-angles. The altitude of the entry interface computed with the overshoot theory is for every test case lower than than the altitude used in the fixed interface method.
Table 4.7 summarises the range of possible entry conditions predicted in the different cases and highlights the difference between re-entry predictions obtained with different area-to-mass ratios. The table reports the mean values and the standard deviations for the different re-entry predictions. The main difference is related to the altitude of the entry interface. Considering an-area to mass ratio associated to the spacecraft with solar panels leads to a mean entry altitude prediction of 99.91 km. If the prediction is instead performed considering an area-to-mass ratio associated only to the main body, the mean interface altitude drops to 95.85 km. The re-entry prediction obtained exploiting the overshoot theory are characterised by a higher standard deviation of the results with respect to the entry conditions obtained assuming a fixed atmospheric interface.
Considering a disposal strategy from HEO, the entry orbit maintains generally a high eccentricity and high energies. The re-entry can be therefore characterised by multiple low altitude passages of the spacecraft in the atmosphere of the Earth that could modify the characteristics of the spacecraft influencing so the re-entry prediction. The high energetic entry conditions imply and atmospheric flight phase that will therefore involve higher mechanical and thermal loads with respect to more standard LEO re-entries. A prediction of the loads acting on INTEGRAL during the entry phase is performed Chapter 5.

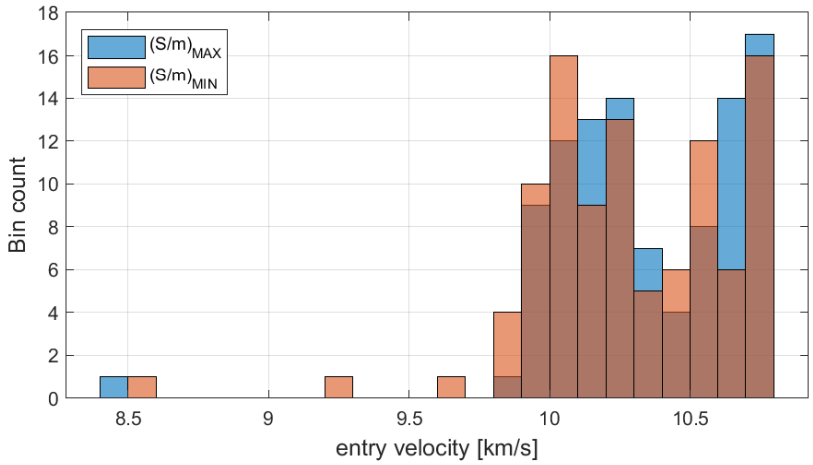

(a)

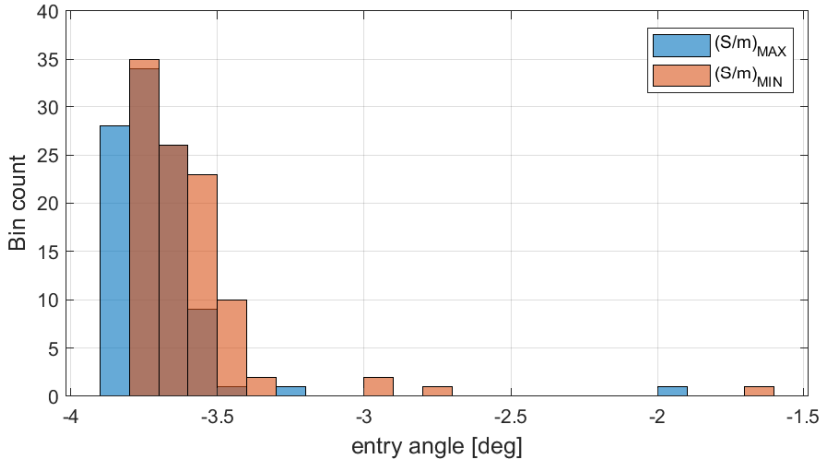

(b)

Figure 4.13: Distribution of the predicted entry velocity (a) and entry angle (b) for 100 test cases obtained exploiting the overshoot boundary theory as interface method. Prediction obtained considering an area-to-mass ratio value with solar panels (blue) and without solar panels (orange).

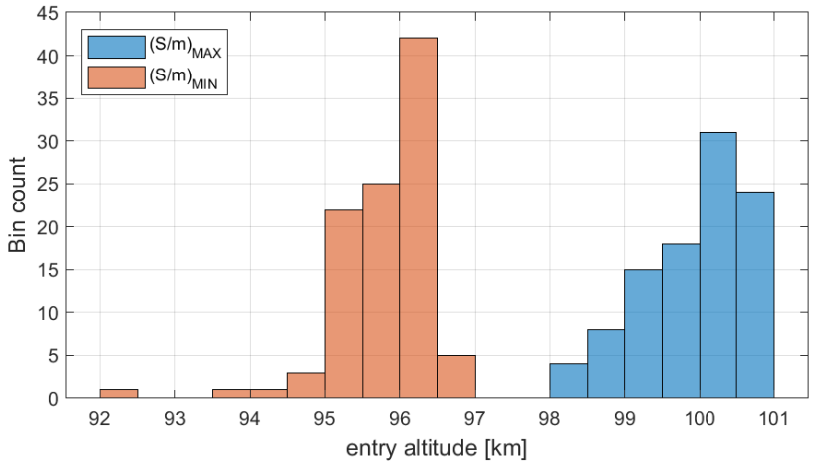

Figure 4.14: Distribution of the predicted entry altitude for 100 test cases obtained exploiting the overshoot boundary theory as interface method. Prediction obtained considering an area-to-mass ratio value with solar panels (blue) and without solar panels (orange).

	fixed interface	**$(S/m)_{MAX}$**	**$(S/m)_{MIN}$**
mean v_e	10.86 [km/s]	10.35 [km/s]	10.28 [km/s]
std. deviation v_e	$\sim$ 0.00 [km/s]	0.34 [km/s]	0.35 [km/s]
mean γ_e	-5.84 [deg]	-3.70 [deg]	-3.60 [deg]]
std. deviation γ_e	$\sim$ 0.00 [deg]	0.21 [deg]	0.25 [deg]
mean h_e	120 [km]	99.91 [km]	95.85 [km]
std. deviation h_e	0 [km]	0.67 [km]	0.65 [km]

Table 4.7: Mean value and standard deviation of the entry velocity v_e, entry angle γ_e and interface altitude h_e for the different re-entry predictions (fixed interface, overshoot theory with $(S/m)_{MAX}$ and overshoot theory with $(S/m)_{MIN}$.

4.5.2 Solar panels break-off

As demonstrated comparing the different entry conditions shown in Figure 4.13 and 4.14, the area of the spacecraft is influencing the re-entry prediction. If the vehicle is equipped with solar panels, the increased mean cross-section area influences both the drag force acting on the spacecraft and the overshoot theory. The re-entry trajectory of the complete vehicle (considering the presence of solar panels) is therefore different from the trajectory of the main body. The distribution of the entry altitudes predicted in Section 4.5.1 shows that the re-entry of the spacecraft is predicted to occur around the same altitude where generally a break-off of the solar panels is verified; therefore, we present an analysis to study the influence of such an occurrence.
In order to produce a more refined estimation of the possible entry trajectories of INTEGRAL , the present section presents the results of the propagation of 500 uncertain test cases considering a break-off of the solar panels if a passage at an altitude below 95 km is present. The distribution of the in-plane and out-of plane angles and of the magnitude of the impulsive velocity variation of the 500 test cases are reported in Figure 4.15. The figures highlights the normal distribution of the random values around the nominal conditions.
The solar panels break-off altitude is selected according to the break-up model used in SESAM and other object-oriented models [44] [46]. The purpose of the computation is to obtain a distribution of the entry characteristics taking into account uncertainty effects and the eventual break-off of the solar panels.
The results of the computation showed that the 10% of the re-entry trajectories are characterised by a perigee passage below 95 km of altitude that lead to a break-off of the solar panels before the entry conditions are met.

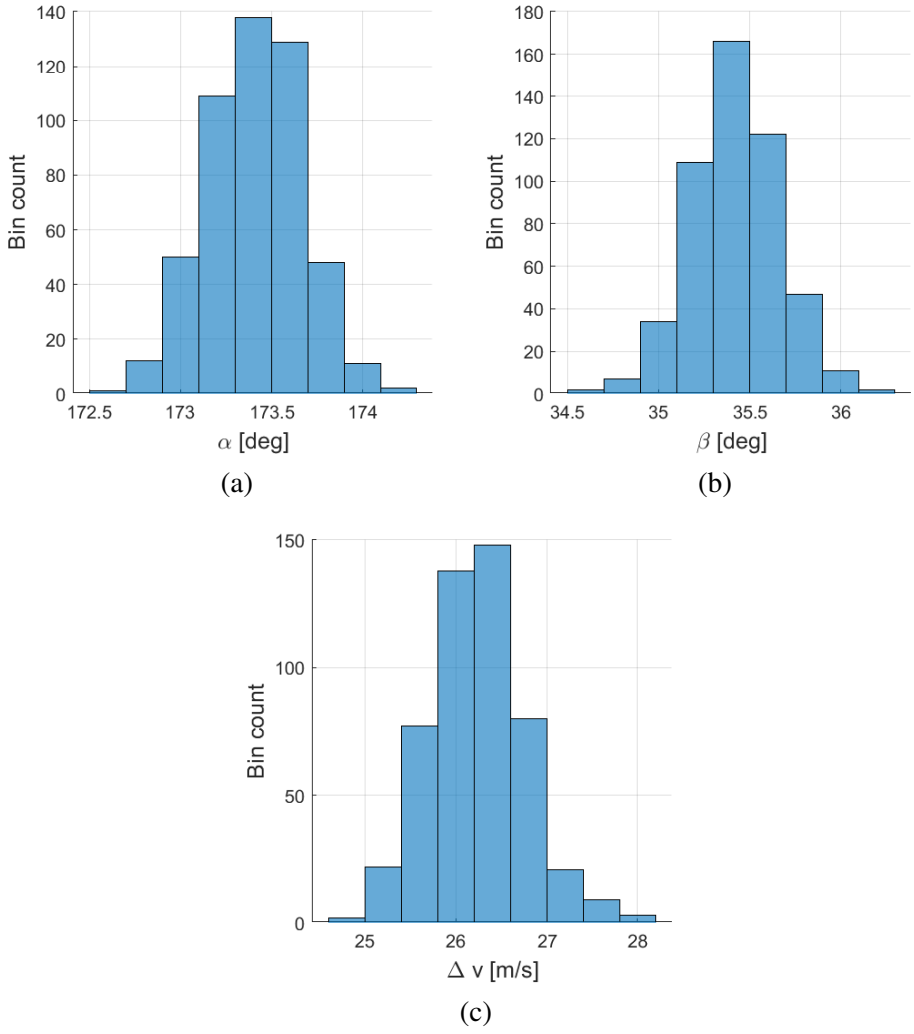

Figure 4.15: Distribution of manoeuvre characteristics considering uncertainties on magnitude and manoeuvre angles: 500 test cases.

The evolution of the entry trajectories is shown in Figure 4.16 and compared with the overshoot boundary. The figure highlights the influence that the uncertainty on the disposal manoeuvre has on the predicted re-entry trajectory. Note that most of the re-entry trajectories are characterised by a high eccentricity that will lead to an atmospheric

flight phase associated to high mechanical and thermal loads.

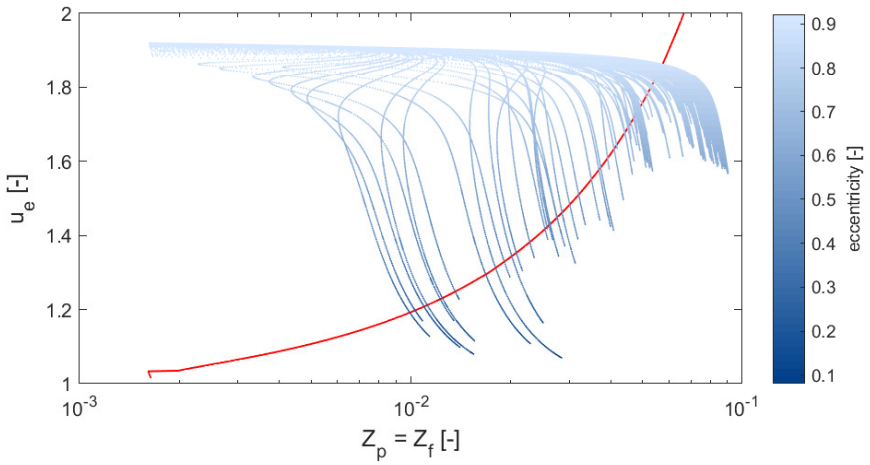

Figure 4.16: Overshoot boundary and evolution of the disposal trajectory for 500 test cases.

The distribution of the entry conditions at the atmospheric interface is reported in Figure 4.17 and 4.18. The figures show the bin count for the test cases divided between trajectories that do not present a break-off of the solar panels before the atmospheric entry (blue) and the cases in which this occurrence is verified (orange).
The results obtained show that a high number of entry trajectories are characterised by entry conditions that appertain at a relatively small range of values. The 86.8% of the cases analysed are characterised by a entry velocity in a range between 10 and 10.8 km/s and the 78.2% have a flight-path angle at the entry interface between -3.8 and -3.5 degrees. It can be noted that some solution present high entry velocity and low entry angles. According to the indications reported in Colombo et al. [11] these entry conditions could lead to the prediction of a skip of the atmospheric entry of the spacecraft.

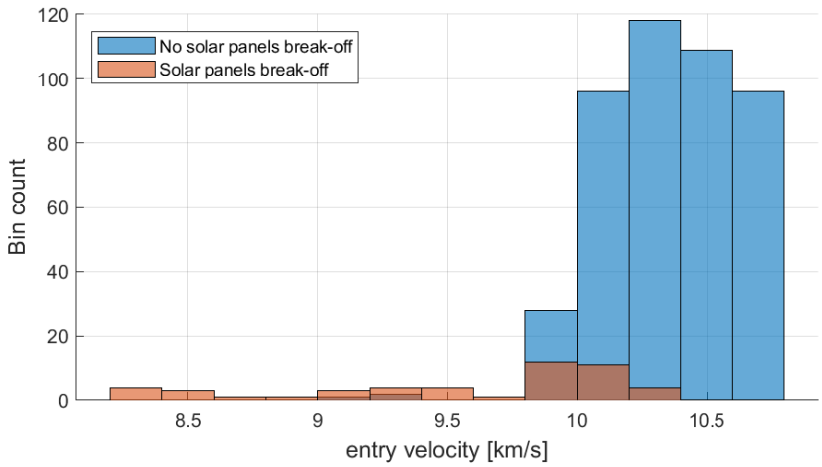

(a)

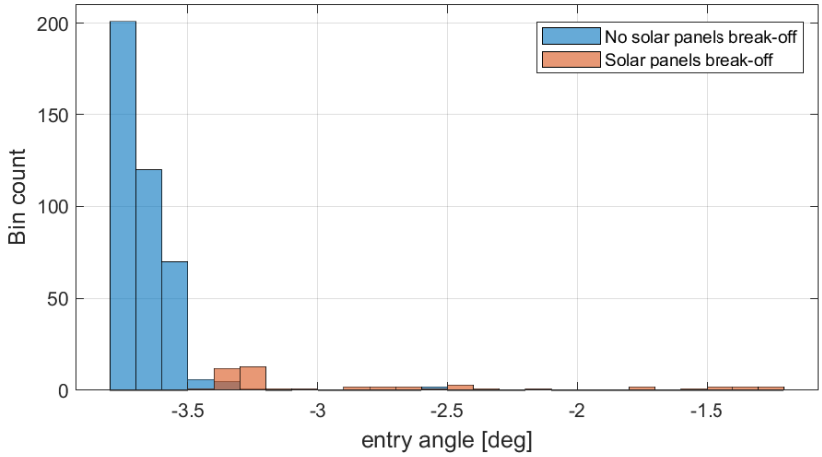

(b)

Figure 4.17: Entry velocity (a) and entry flight-path angle (b) for 500 test cases obtained exploiting the overshoot boundary theory as interface method and considering a solar panels break-off at 95 km of altitude.

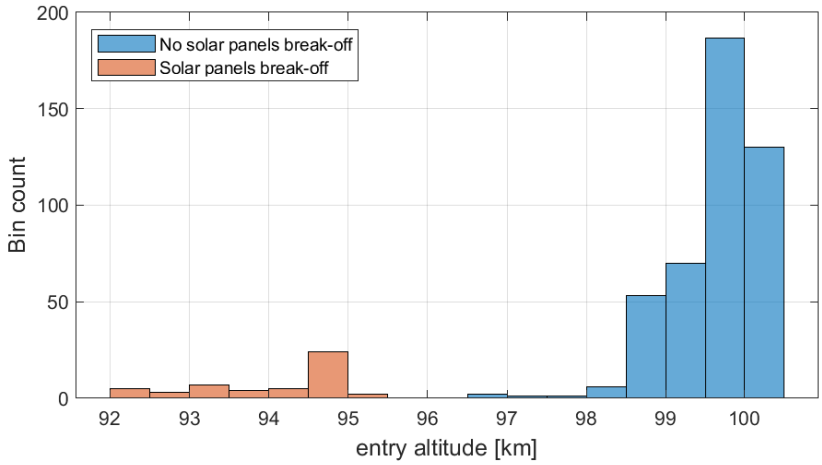

Figure 4.18: Entry altitude for 500 test cases obtained exploiting the overshoot boundary theory as interface method and considering a solar panels break-off at 95 km of altitude.

Figure 4.19 shows the average number of low altitude passages (below 120 km) performed by the spacecraft before reaching the entry conditions, as function of the perigee altitude of the re-entry orbit. The figure shows that the trajectories that are associated to an early break-off of the solar panels are also characterised by a higher number of atmospheric passages before the re-entry. A higher number of low altitude passages leads to entry orbits with lower eccentricities and higher pericenter altitudes. Note that, according to the considerations reported in Trisolini et al. [30], the drag effect acting on the spacecraft, responsible of the circularisation of the orbit, could also produce thermal and mechanical loads high enough to produce an early fragmentation of the vehicle. The final part of the entry trajectory can be analysed assuming that no early breakup of the spacecraft is verified until the entry conditions are met. The final leg of the disposal strategy assuming planar motion and no lift is analysed in the next chapter.
The average values of the entry altitude, entry velocity and flight-path angle for 500 test cases are summarised in Table 4.8.

The possible entry conditions obtained here will be used in Chapter 5 to perform an estimation of mechanical and thermal loads acting on INTEGRAL during the re-entry.

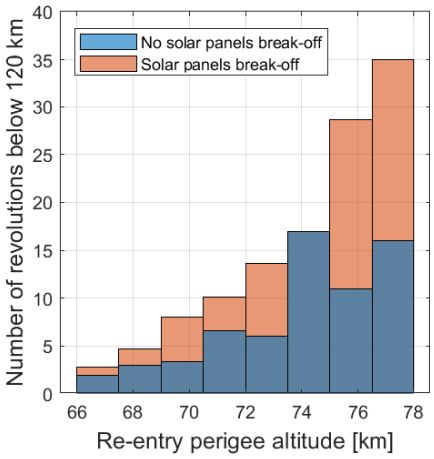

Figure 4.19: Average number of revolutions with low altitudes passages (below 120 km).

	No solar panels break-off	**Solar panels break-off**	**Complete set of data**
Number of cases	450/500	50/500	500/500
v_e	10.36 [km/s]	9.52 [km/s]	10.28 [km/s]
γ_e	-3.68 [deg]	-2.74 [deg]	-3.59 [deg]
h_e	99.66 [deg]	94.12 [km]	99.10 [km]

Table 4.8: Average entry conditions.

Chapter 5

Atmospheric flight

The final part of the disposal trajectory is computed according to the atmospheric entry conditions obtained in the previous section, taking into account a possible break-off of the solar panels before the re-entry. The possible entry characteristics are used to perform an estimation of the atmospheric flight of the satellite.

5.1 Final leg

The equations of motion that model the trajectory of a spacecraft entering the atmosphere of a celestial body can be written considering the rotation of the planet. The motion of the entering vehicle can be widely simplified assuming planar motion over a non-rotating planet. In the case of the Earth, the values of the inertial and the relative velocity vector differ by a westward-pointing vector of magnitude of almost $463 \cos \lambda$ m/s at sea level, where λ is the latitude of the spacecraft. As reported in Ashley [47] the errors due to neglecting the planet rotation are in most case of interest less than 10 percent. The atmospheric flight phase of the re-entry trajectory of INTEGRAL is therefore here described assuming planar motion and no lift in a non-rotating environment [11][48] according to the following equations

$$\begin{aligned}
\frac{dv}{dt} &= -\frac{\rho(h)}{2B}v^2 + g(h)\sin\phi \\
v\frac{d\phi}{dt} &= \cos\phi\left(g(h) - \frac{v^2}{R_E + h}\right) \\
\frac{dh}{dt} &= -v\sin\phi \\
\frac{dx}{dt} &= v\cos\phi
\end{aligned} \tag{5.1}$$

where B is the ballistic coefficient, v is the inertial velocity magnitude, ϕ is the opposite of flight-path angle (γ), h is the altitude of the spacecraft and x is the downrange. The ballistic coefficient is defined as

$$B = \frac{m}{C_D A} \tag{5.2}$$

The trajectory is computed solving the set of differential equations defined by Eqs.(5.1) using as initial conditions the the atmospheric entry conditions obtained in Section 4.5.2 using the overshoot theory reported in Chapter 3. The gravity term is defined with an inverse square central gravity term and the atmospheric density is again described with a strictly exponential model, according to the approximations adopted in the overshoot boundary theory.
Figure 5.1 and Figure 5.2 show the final leg of the 500 re-entry trajectories of INTEGRAL obtained considering uncertainties on the disposal manoeuvre and taking into account a possible solar panels break-off before the predicted re-entry. The black lines show the predicted re-entry considering a fixed altitude of 120 km for the interface between the long-term propagation and the atmospheric entry. Recall that in this case the initial conditions are related to a long-term evolution per-

formed neglecting the drag effect. The trajectory is compared with the results obtained computing the entry conditions with the overshoot boundary theory obtained in Section 4.5.2. In this case the long-term propagation considers the effect of atmospheric drag.
Figure 5.1 shows the effects of a manoeuvre uncertainty on the predicted re-entry. Entry trajectories predict a time to ground in a range between ∼580 and ∼1860 with a maximum downrange of more than 11000 km.
Note that in general the overshoot theory predicts a slower re-entry (with respect to the fixed altitude interface) with lower entry flight-path angles. The re-entry from HEO is characterised by high energy and is predicted to occur close to the perigee, at low entry flight-path angles. For this reason the integration of the equations reported above can produce trajectories that present a bounce of the spacecraft on the upper layer of the atmosphere.
Figure 5.2 shows the trend of the velocity magnitude and the flight-path angle during the atmospheric flight. Due to the lower entry angles, the results predicted with the overshoot theory are characterised by a later deceleration. The results are in agreement with the consideration that, due to the low initial flight-path angles, the time required to reach the thickest atmospheric layers present at low altitudes is increased.

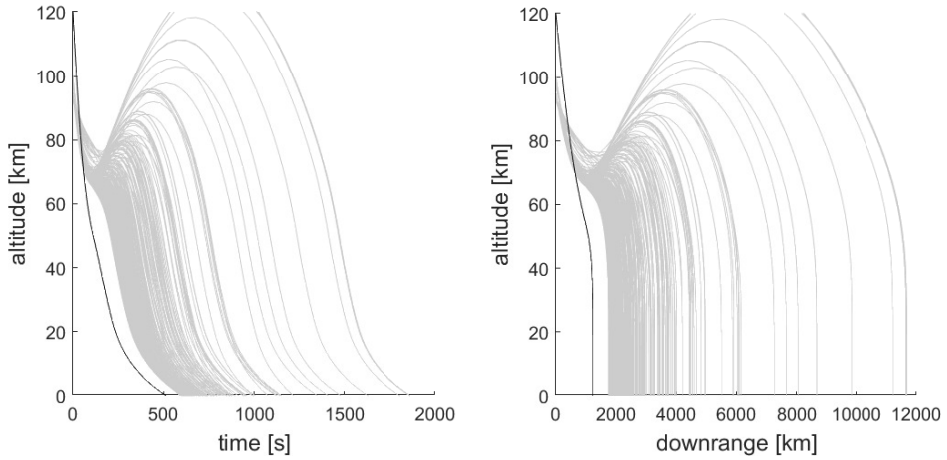

(a) (b)

Figure 5.1: Predicted evolution of the altitude of INTEGRAL with respect to time (a) and downrange (b). Comparison between re-entry estimation obtained with a fixed atmospheric interface (black line) and estimation with the overshoot boundary theory (grey lines).

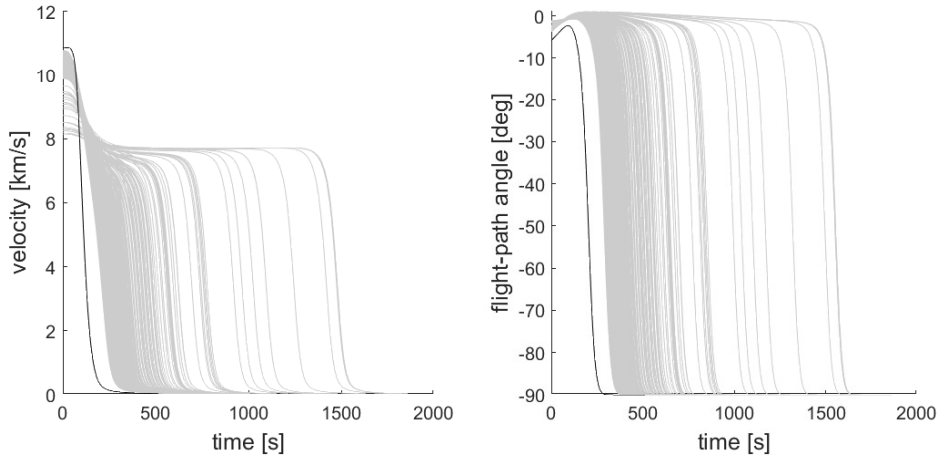

(a) (b)

Figure 5.2: Predicted evolution of velocity (a) and flight-path angle (b) using a fixed interface altitude (black line) and the overshoot boundary (grey lines) theory as interface methods.

5.2 Mechanical and thermal loads

The entry conditions obtained show that, even if drag effects are considered, the entry velocity of a disposal strategy from HEO is usually much higher than the typical entry velocity from LEO.
When the spacecraft enters the atmosphere with high velocity, the kinetic energy is converted into thermal energy and partially dissipated in the environment. The thermal and mechanical loads acting on the vehicle during the atmospheric flight phase are responsible of the fragmentation of the spacecraft. For this reason the present chapter is focused on the estimation of the loads acting on INTEGRAL once the entry conditions are met. When the entry trajectory is defined, a preliminary estimation of the mechanical and thermal loads acting on the spacecraft during the atmospheric phase of the re-entry is obtained solving the following equations [11] [19]

$$n = \frac{1}{g_0}\left|-\frac{D}{m} + g(h)\sin\phi\right| \tag{5.3}$$

$$q = C_D\frac{\rho(h)v^3}{2} \tag{5.4}$$

where g_0 is the ground level gravitational acceleration and

$$D = \frac{1}{2}\rho(h)v^2 C_D A \tag{5.5}$$

The equations reported above can be used to perform a quick comparison between different re-entry conditions.
The data relative to the uncertainty analysis over 500 test cases produced in Chapter 4 and reported in Figure 4.17 and 4.18 are used to

extract the limit values that define the atmospheric flight of the spacecraft.

Figure 5.3 and 5.4 show the trend of the mechanical and thermal loads acting on the spacecraft during the re-entry phase. For the clarity of the images only a subset of 50 of the 500 cases analysed (grey lines) are depicted in the figures.

Figure 5.3 shows the trend of the mechanical load acting on INTEGRAL during the re-entry expressed as ratio with the ground level acceleration. It can be noted that the prediction obtained with the overshoot theory (grey lines) are characterised by a lower maximum load factor with respect to the estimation performed with the fixed interface (black line). A lower entry angle implies a general lower maximum load factor. The entry conditions computed with the overshoot theory predict a slower re-entry that implies a lower altitude for the maximum acceleration. The figure shows the trajectories associated to the maximum (red) and minimum (blue) peak mechanical load obtained during the atmospheric flight phase. The trend shows that an uncertainty of 2% on the magnitude of the velocity manoeuvre and of 0.25 degrees on the manoeuvre angles produces an uncertainty of around 2 g on the peak acceleration experienced by the vehicle during the re-entry. The altitude at which the spacecraft is experiencing the peak deceleration does not undergo great variations.

The trend of the thermal flux density is computed according to Eq.(5.4) and reported in Figure 5.4.

The fixed interface method is characterised by a thermal flux density acting on the spacecraft during the re-entry that reaches a peak value at an altitude around 56 km. The predicted trend of the thermal flux density computed exploiting the overshoot boundary as interface method is instead characterised by a different behaviour, reaching a peak value for two different altitudes. A first maximum is in most of the cases reached around 70 km of altitudes and a second global maximum value is computed for an altitude around 50 km. The two peaks of the ther-

mal flux density are related to the trend of most of the trajectories that present a first decrease of the altitude followed by a new ascent phase. The effect of the uncertainty on the thermal flux density are analysed in Section 5.3 in order to obtain an estimation of the break-up process and to define a range of the possible altitudes of fragmentation of the spacecraft.

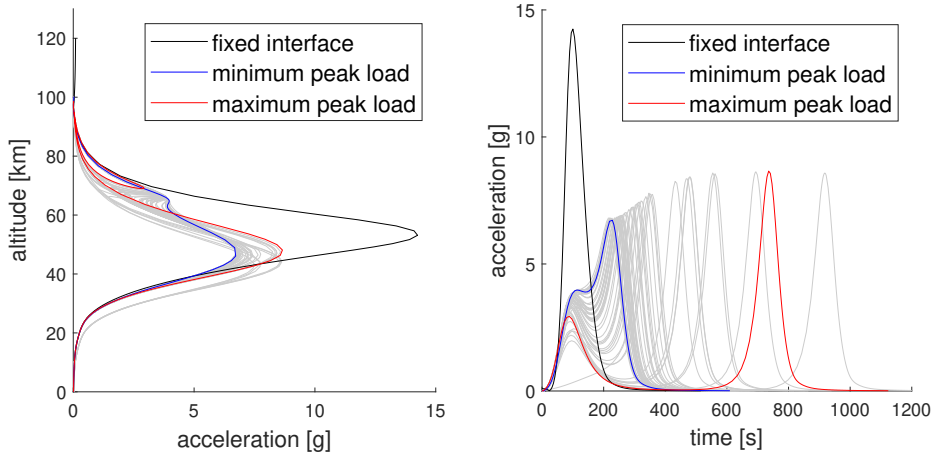

Figure 5.3: Predicted evolution of the mechanical load acting on INTEGRAL with respect to altitude (a) and time (b) from the entry instant. Trajectories associated to the maximum (red line) and minimum (blue line) peak mechanical accelerations.

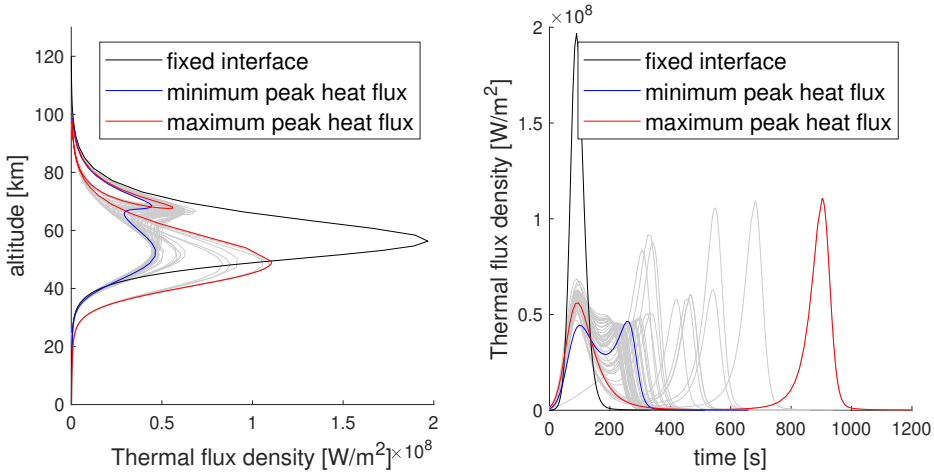

(a) (b)

Figure 5.4: Predicted evolution of the thermal flux density acting on INTEGRAL with respect to altitude (a) and time (b) from the entry instant. Trajectories associated to the maximum (red line) and minimum (blue line) peak thermal flux density.

5.3 Break-up altitude

The trend of thermal flux density reported in Figure 5.4 is used to obtain the variation of the temperature of the spacecraft during the re-entry phase. The temperature variation is obtained assuming that the main structure of the satellite is constituted of Aluminum alloy. The estimation of the break-up altitude is then performed comparing the temperature trend during the re-entry and the melting point of the material of the structure. The estimation is performed assuming a structural mass of the satellite of 1200 kg and a initial temperature (temperature at the entry interface) of 300 K.
The distribution of the break-up altitude of 500 test cases considering uncertainties in the disposal manoeuvre is reported in Figure 5.5. Even if the entry conditions computed cover a wide range of possible entry trajectories, with some solution leading to a possible entry skip, all the solution reach the melting temperature in the first descending part of the trajectory and they are all characterised by a similar break-up altitude. All the re-entry trajectories are indeed characterised by a break-up altitude between 77.5 and 82.5 km with a mean value of the distribution of 80.11 km. The results obtained are in agreement with the typical break-up altitudes assumed in object-oriented methods [44]. Note that the procedure is based on a very simplified model of the spacecraft and the method adopted to estimate the break-up altitude is highly influenced by the mass and the material associated to the structure of the satellite.
The analysis neglects also possible aerothermodynamic effects associated to low altitude passages of the spacecraft before the instant when the atmospheric capture is verified that could modify the geometry of the spacecraft. The computation relies on the assumption that the structure and the configuration of the spacecraft remain unchanged until the re-entry conditions obtained with the overshoot theory are met. It must therefore be considered that the results obtained are a rough

estimation of the destructive process.

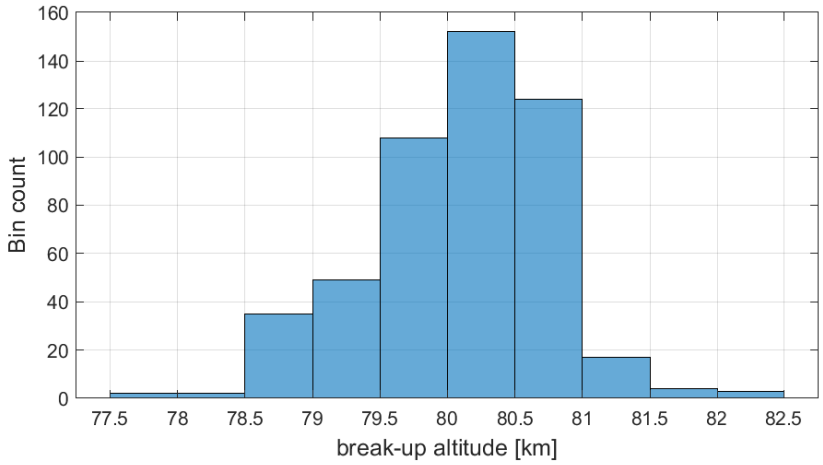

Figure 5.5: Predicted break-up altitude

5.4 Re-entry overview

All the initial conditions at the entry interface obtained exploiting the overshoot theory as interface method define reasonable atmospheric trajectories. Particular entry conditions lead to a trajectory estimation characterised by a new increase of the altitude of the spacecraft before the ground impact is verified. Despite the presence of this solutions the break-up analysis based on a simplified model of the spacecraft demonstrated that every entry trajectory leads to a fragmentation of the satellite in the first part of the re-entry. The solutions characterised by very low entry flight-path angles affect the predictions of maximum downrange and time to ground.
The estimation of the mechanical loads acting on the spacecraft showed that all the solutions present a peak mechanical load between 6.71 and 8.66 g at an altitude of $\sim$ 50 km according to the results obtained considering a fixed interface.
The simplified estimation of the break-up altitude demonstrated that despite the possible entry conditions are distributed over a wide range of possibilities, all the trajectories are characterised by a similar breakup altitude with a mean value of the distribution of 80.11 km.
The boundaries that define the atmospheric entry considering a manoeuvre affected by possible uncertainties as defined in Section 4.5 are summarised in Table 5.1.

	Minimum	**Maximum**
Time to ground	592 [s]	1863 [s]
Peak acceleration	6.71 [g]	8.66 [g]
Breakup altitude	77.5 [km]	82.5 [km]

Table 5.1: Integral: re-entry limits

Chapter 6

Conclusions and future applications

The aim of this thesis was to produce an approach to analyse efficiently the re-entry strategy of a satellite from Highly Elliptical Orbits. The disposal strategy analysed in this work exploits the luni-solar perturbative effects to obtain a long-term natural re-entry of the spacecraft. The re-entry is achieved with entry velocities that are much higher than typical entry velocities that characterise re-entries from Low Earth Orbits. The analysis performed in this thesis demonstrated that the overshoot theory presented by Hicks [1] defines a reliable method to estimate the conditions that allow the spacecraft to achieve a proper atmospheric entry. The model provides a method to interface the long-term propagation and the destructive re-entry phases and to obtain therefore a quick estimation of the complete re-entry trajectory.

The re-entry estimation produced in this work is consistent with the results obtained in other studies about re-entering objects [30]. In particular the results obtained with this more refined model agree with the entry estimation performed considering a fixed altitude for the entry interface [11].

The analysis performed taking into account possible uncertainties on

the disposal manoeuvre demonstrated the main differences between the re-entry estimation performed considering a fixed interface altitude (and neglecting drag) and and the entry conditions obtained exploiting the overshoot theory. The comparison between the two methods showed that the re-entry estimation performed exploiting the overshoot theory leads the possible entry conditions to cover a larger range. Considering a fixed interface leads instead to possible entry conditions characterised by a very low standard deviation. The effect of atmospheric drag is therefore responsible of an extension of the range of the possible entry conditions. Exploiting the overshoot theory allows us therefore to perform a comparison between the destructive phase of different re-entry strategies keeping a low computational cost.

The analysis performed in Section 4.4 proved that several passages in the atmosphere of the Earth are needed by the spacecraft to reach entry conditions. High-velocity atmospheric passages that characterise the re-entry from Highly Elliptical Orbits could be responsible of the generation of mechanical and thermal loads able to produce a fragmentation of the spacecraft before the re-entry, implying a possible release of components of the vehicle in orbit. Re-entries affected by a higher circularisation should therefore be avoided. The results shown in Figure 4.19 demonstrated that the number of revolutions with low altitudes and an early break-off of the solar panels are events strictly connected to each other. In order to avoid a possible release of space debris in orbit, the design of the disposal trajectory should target steep re-entries.

Averaged techniques allow us to obtain the evolution of the orbital elements over a long-term in few seconds. The model developed in this work can be therefore easily used to perform a comparison between a high number of long-term disposal strategies. The entry conditions of re-entry trajectories can be obtained rapidly and can be used to perform a quick estimation of the loads acting on the spacecraft during the atmospheric flight phase. The trend of the thermal loads can be used

in combination with a simplified model of the spacecraft to produce an evaluation of the altitude of fragmentation of the spacecraft, providing a tool to compare re-entry strategies. Due to the low computational time the method can be used in a preliminary design phase of end-of-life manoeuvres to identify optimal solution ranges.

Even if the model seems good enough to face the estimation of a disposal strategy, several improvements of the model could be included. It is important to note that both the atmospheric and the gravity model used in this work are simple approximations of complex fields. The atmospheric model used in this work is designed to fit a defined altitude range and is not considering possible density variations due to solar activities. In order to improve the accuracy of the model the exponential atmospheric model could therefore be replaced with a more refined one. As recommended in Hicks [1] a reasonable replacement can be the 1962 Standard Atmosphere model. The gravity field is in the overshoot theory approximated with an inverse square central gravity term and the effects of the oblateness of the Earth are considered only in the long-term orbit propagation. A possible method to produce a more refined model could be to include the effects related to the asymmetry of the gravity field of the Earth also in the re-entry estimation.

Future improvements might be also focused on the enhancement of the aerodynamic model. During the re-entry in the atmosphere of the Earth the space vehicle encounters free-molecular, transition and continuum regime. A proper value of the drag coefficient of the entering object should be selected depending on the flow regime. In this work the drag coefficient is considered constant in the unified theory of the overshoot boundary, with the purpose to use the same approximation used in the long-term propagation. According to the equations presented in Section 4.3.2 the drag coefficient could be defined as function of the Knudsen number in order to consider the different flow regimes encountered at different altitudes.

The model adopted for the estimation of the break-up altitude repre-

sents only a simplified prediction of the destructive phase that could be used to compare the effectiveness of different strategies. A more refined analysis of the destructive phase should be performed, with the intent of verifying the compliance of the disposal strategy with the safety requirements. The procedure adopted in this work to perform the re-entry prediction can be used to interface the long-term orbital propagation with a object-oriented code to obtain a preliminary estimation of the demisability of the spacecraft during the re-entry in the Earth's atmosphere. The method could so be used to perform the optimization of the disposal strategy based on the prediction of the risks associated to the re-entry, the residual mass fraction of the satellite impacting on ground and other parameters. An approach that couples the long-term propagation and an object-oriented model could so be used to identify the trajectories that allow a proper demise of the most critical components of the spacecraft during the re-entry phase. The solution found interfacing the averaged long-term orbit propagation with the atmospheric flight analysis provides a method for the preliminary design of a disposal manoeuvre.

Bibliography

[1] Kerry D. Hicks. *Introduction to Astrodynamic Reentry*. Books Express Publishing, 2009.

[2] ESA website. *Integral*. 2019. URL: https://sci.esa.int/s/wxDX1vw.

[3] M. L. Lidov. "Evolution of the orbits of artificial satellites of planets as effected by gravitational perturbation from external bodies". In: *AIAA Journal* 1.8 (Aug. 1963).

[4] Y. Kozai. "On the effects of the sun and the Moon upon the Motion of a close Earth satellite". In: *SAO Special Report* 22.2 (Mar. 1959).

[5] "Lidov Michail L'vovich (1926-1993)". In: *Astronomy Letters* 20.3 (May 1994).

[6] Yoshihide Kozai. "A new method to compute Luni-solar perturbations in Satellite motion". In: *SAO Special Report* 349 (Feb. 1973).

[7] G. E. Cook. "Luni-Solar perturbations of the Orbit of an Earth Satellite". In: *Geophysical Journal International* 6.3 (Apr. 1962), pp. 271–291. DOI: https://academic.oup.com/gji/article/6/3/271/650378.

[8] I.V.d. Costa and A.F.B.d.A. Prado. "Orbital Evolution of a Satellite perturbed by a third body". In: *Advances in Space Dynamics* (2000).

[9] Desmond King-Hele. *Theory of satellite orbits in an atmosphere*. Butterworths Mathematical Texts, 1964.

[10] Bernard Kaufman and Robert Dasenbrock. *Higher order theory for long-term behavior of earth and lunar orbiters*. Tech. rep. NAVAL RESEARCH LAB WASHINGTON DC OPERATIONS RESEARCH BRANCH, 1972.

[11] C. Colombo et al. “End-of-life re-entry for highly elliptical orbits: the INTEGRAL mission”. In: *Advances in the Astronautical Sciences* (Jan. 2014). DOI: http://hdl.handle.net/11311/943363.

[12] C. Colombo. “Long-term evolution of highly-elliptical orbits: luni-solar perturbation effects for stability and re-entry”. In: *Frontiers in Astronomy and Space Sciences* 6 (2019), p. 34. DOI: 10.3389/fspas.2019.00034.

[13] C. Colombo. “Planetary Orbital Dynamics (PlanODyn) Suite for long term propagation in perturbed environment”. In: *6th International Conference on Astrodynamics Tools and Techniques (ICATT). Darmstadt, Germany* (Mar. 2016), pp. 14–17.

[14] National Aeronautics and Space Administration. *Handbook for Limiting Orbital Debris*. 2008.

[15] ESA Space Debris Mitigation WG. *ESA Space Debris Mitigation Compliance Verification Guidelines*. ESA. Feb. 2015.

[16] F. Alby et al. “The European Space Debris Safety and Mitigation Standard”. In: *Advances in Space Research* 34.5 (2004), pp. 1260–1263. DOI: https://doi.org/10.1016/j.asr.2003.08.043..

[17] ESA. *Space Environment Statistics*. 2021. URL: https:https://sdup.esoc.esa.int/discosweb/statistics/.

[18] C. Colombo, E.M. Alessi, and M. Landgraf. “End-of-life disposal of spacecraft in Highly Elliptical Orbits by menas of luni-solar perturbations and Moon resonances”. In: *6th European Conference on Space Debris* 6.1 (Apr. 2013).

[19] S. M. Anandakrishnan F. J. Reagan. *Dynamics of atmospheric re-entry*. AIAA, 1993.

[20] C. Colombo. “Long-term evolution of highly-elliptical orbits: luni-solar perturbation effects for stability and re-entry”. In: *Proceedings of the 25th AAS/AIAA Space Flight Mechanics Meeting*. AAS-15–395, Williamsburg. 2015.

[21] R. Armellin, J.F. San-Juan, and M. Lara. "End-of-life disposal of high elliptical orbit missions: the case of INTEGRAL". In: *Advances Space Research* 56.3 (Aug. 2015), pp. 365–582. DOI: https://doi.org/10.1016/j.asr.2015.03.020..

[22] D. Mistry and R. Armellin. "The Design and Optimisation of End-of-life Disposal manoeuvres for GNSS Spacecraft:The case of Galileo". In: *66th International Astronautical Congress. Jerusalem, Israel* (2015). URL: https://surrey.eprints-hosting.org/840752/.

[23] K. Merz et al. "Orbit Aspects of End-Of-Life Disposal from Highly Eccentric Orbits". In: *International Symposium on Space Flight Dynamics* (2015).

[24] T. Lips and B. Fritsche. "A comparison of commonly used re-entry analysis tools". In: *Acta Astronautica* 57.2-8 (2005), pp. 312–323.

[25] J. Beck et al. "Progress in hybrid spacecraft7object oriented destructive reentry modelling using the SAM code". In: *7th European Conference on Space Debris. Darmstadt, Germany* 7.1 (2017).

[26] M.A. Weaver, R.L. Baker, and M.V. Frank. "Probabilistic estimation of reentry debris area". In: *3rd European Conference on Space Debris, ESOC. Darmstadt, Germany* 473 (2001), pp. 515–520.

[27] M. Trisolini, H.G. Lewis, and C. Colombo. "Demise and survivability criteria for spacecraft design optimisation". In: *Journal of Space Safety Engineering* 3.2 (2016), pp. 83–93.

[28] M. Trisolini. "Space system design for demise and survival". PhD thesis. University of Southampton, 2018.

[29] M. Trisolini, H.G. Lewis, and C. Colombo. "Spacecraft design optimisation for demise and survivability". In: *Aerospace Science and Technology* 77 (2018), pp. 638–657.

[30] M. Trisolini and C. Colombo. "Demisability analysis of re-entering structures on resonant trajectories". In: *5th International Space Debris Re-entry Workshop* 1.1 (2020).

[31] H.D. Curtis. *Orbital Mechanics for Engineering Students*. Elsevier, 2015.

[32] D.A. Vallado. *Fundamentals of Astrodynamics and Applications*. McGraw-Hill, 1997.

[33] R.H. Battin. *An introduction to he Mathematics and Methods of Astrodynamics*. Education Series, 1999.

[34] P. Fortescue. *Spacecraft Systems Engineering*. Wiley, 2011.

[35] Space Research Blog. *Orbit Perturbations Magnitude*. 2020. URL: https://spaceresearch.top/blog/19f77bd6/.

[36] C. Colombo. "Optimal trajectory design for interception and deflection of Near Earth Objcets". English. PhD thesis. University of Glasgow, 2010.

[37] F. Scala. "Analytical design of End-of-life disposal manoeuvres for Highly Elliptical Orbits under the influence of the third body's attraction and planet's oblateness". MA thesis. Politecnico di Milano, 2018.

[38] ESA. *Mitigating Space Debris Generation*. 1999. URL: https://www.esa.int/Safety_Security/Space_Debris/Mitigating_space_debris_generation.

[39] N. X. Vinh, A. Busemann, and R.D. Culp. *Hypersonic and Planetary Entry Flight Mechanics*. The University of Michigan Press, 1980.

[40] ESA. *Summary*. 2019. URL: https://sci.esa.int/web/integral/-/31149-summary.

[41] Alenia Aerospazio. *INTEGRAL Critical Design Review CDR*. 1999. URL: https://www.cosmos.esa.int/web/integral/spacecraft-drawings.

[42] R.D. Klett. *Drag coefficients and heating ratios for right circular cylinders in free molecular and continuum flow from Mach 10 to 30*. Tech. rep. Sandia Corp., Albuquerque, N. Mex., 1964.

[43] M. Trisolini, H.G. Lewis, and C. Colombo. "Demisability and survivability sensitivity to design-for-demise techniques". In: *Acta Astronautica* 145 (2018), pp. 357–384.

[44] J.Gelhaus et al. "Upgrade of DRAMA, ESA' s Space Debris Mitigation Analysis Tool Suite". In: *6th European Conference on Space Debris. Darmstadt, Germany* (2013).

[45] G. Bélanger and C. Winkler. *INTEGRAL Announcement of Opportunity for Observing Proposals (AO-7)*. 2009.

[46] Hyperschall Technologie Goettingen Gmbh. *Final Report, Upgrade of DRAMA's Spacecraft Entry Survival Analysis Codes*. Tech. rep. European Space Agency, Dec. 2018.

[47] H.Ashley. *Engineering Analysis of Flight Vehicles*. Dover Publications, 1974.

[48] T. Rivell. *Notes on Earth Atmospheric Entry for Mars Sample Return Missions*. Tech. rep. Ames Research Center, Moffett Field, California, 2006.